

Lattice models of random advection and diffusion and their statistics

Stefano Lepri ^{1,2} Paolo Politi ^{1,2} and Arkady Pikovsky ³

¹Consiglio Nazionale delle Ricerche, Istituto dei Sistemi Complessi, Via Madonna del Piano 10, I-50019 Sesto Fiorentino, Italy

²Istituto Nazionale di Fisica Nucleare, Sezione di Firenze, via G. Sansone 1, I-50019 Sesto Fiorentino, Italy

³Department of Physics and Astronomy, University of Potsdam Karl-Liebknecht-Strasse 24/25, Bldg 28 D-14476, Potsdam, Germany



(Received 5 June 2023; revised 18 September 2023; accepted 9 October 2023; published 31 October 2023)

We study in detail a one-dimensional lattice model of a continuum, conserved field (mass) that is transferred deterministically between neighboring random sites. The model belongs to a wider class of lattice models capturing the joint effect of random advection and diffusion and encompassing as specific cases some models studied in the literature, such as those of Kang-Redner, Kipnis-Marchioro-Presutti, Takayasu-Taguchi, etc. The motivation for our setup comes from a straightforward interpretation of the advection of particles in one-dimensional turbulence, but it is also related to a problem of synchronization of dynamical systems driven by common noise. For finite lattices, we study both the coalescence of an initially spread field (interpreted as roughening), and the statistical steady-state properties. We distinguish two main size-dependent regimes, depending on the strength of the diffusion term and on the lattice size. Using numerical simulations and a mean-field approach, we study the statistics of the field. For weak diffusion, we unveil a characteristic hierarchical structure of the field. We also connect the model and the iterated function systems concept.

DOI: [10.1103/PhysRevE.108.044150](https://doi.org/10.1103/PhysRevE.108.044150)

I. INTRODUCTION

Advection and diffusion are two basic transport phenomena occurring in diverse physical contexts. The former amounts to the motion of, for instance, small tracer particles (such as a pollutant) transported by the movement of a surrounding fluid. On the other hand, diffusion is caused by the familiar mechanism of a Brownian random walk that causes a stochastic spreading of tracer particles due to the interaction with a solvent.

A particularly interesting case is one in which advection is a random process. In the applications to turbulence, there is a vast literature on the matter [1]. A celebrated example is the Kraichnan model for the advection of a passive scalar by a random flow [2]. In this case, one usually assumes an incompressible (solenoidal) velocity field [2] or a weakly compressible fluid [3]. As is known, the former case is related to Hamiltonian dynamical systems theory, as exemplified by Lagrangian chaos [4]. On the other hand, the issue of compressible fluids is less studied and corresponds to dissipative phase-space flows.

In addition to the problem of passive scalar transport in fluids, the concept of advection is more general and applies in a more abstract sense to the spreading of an ensemble of trajectories in phase space of a dynamical system subject to a common regular or irregular phase velocity field. Examples of this setup occur in neurosciences and other fields. Another interesting application concerns transport in active media [5] as it occurs for light in disordered and amplifying systems [5,6].

Mathematically, a description of the problem in the continuum limit requires dealing with a stochastic partial differential equation, but such equations are notoriously hard to deal with. From a more statistical-mechanics point of view, it is thus

helpful to consider simple *discrete* microscopic or mesoscopic models of the dynamics that possess some fundamental features of the problem. Such an approach is insightful as it allows us to simulate the process straightforwardly. In this work, we follow this strategy to take a fresh look at the problem when random advection and diffusion are *both* present. We introduce a general class of stochastic lattice models in which microscopic moves mimic the two basic mechanisms, namely the collective random motion of particles induced by the common advecting field, and the spreading caused by microscopic diffusion (this distinction will be made clear in the following). For simplicity, we deal with a one-dimensional lattice. Discrete dynamics is easily generalized to higher dimensions or graphs, although in these cases a relation to the original continuous advection setup becomes nontrivial (see the discussion in Sec. VIII). We anticipate that this class will encompass various models considered previously in the literature as particular cases.

The primary model we are going to study depends on a single parameter ϵ confined to the unitary interval $[0, 1]$ and allowing for tuning the relative importance of advection and diffusion. This parameter quantifies the fraction of mass which is transferred from a random site to a random neighbor. In one limit ($\epsilon = 0$), there is a whole transfer of mass and the process is characterized by macrodiffusion (or random advection). In the opposite limit ($\epsilon \rightarrow 1$), a vanishing piece of matter is transferred and the process is characterized by microdiffusion. For general ϵ , both processes are present.

We are interested in both the time dependence of the field evolving from an initial uniform state and in the properties of the statistically stationary state that emerges at large times. In the former case, the typical phenomena are coarsening and roughening, namely how clusters merge and how the field variance grows in time. Also, the steady-state statistics of the

field is of great interest. We will report cases in which the statistics is strongly non-Gaussian, and we will be able to give a scaling description of the asymptotic state for any ϵ and any size L of the system.

This paper is organized as follows. In Sec. II we describe the basic phenomenology of advection and diffusion in a smooth, random field, and we introduce the basic distinction between macroscopic (collective) and microscopic diffusion. The general class of models with stochastic microscopic dynamics is defined in Sec. III, and particular cases corresponding to various systems studied in the literature are examined. Our analysis starts by considering the case of no microscopic diffusion for a finite lattice (Sec. IV) and its roughening properties. We then focus on various steady-state properties in Secs. V, VI, and VII. Conclusions are given in Sec. VIII, along with a brief comparison of our results with those given in the literature for other models with similar conservation laws. Some more technical aspects are relegated to the Appendixes.

II. PHENOMENOLOGY OF RANDOM ONE-DIMENSIONAL ADVECTION AND DIFFUSION

Let us start by discussing general qualitative concepts about one-dimensional random passive scalar advection. The starting point is an ensemble of “particles” with coordinates $x_i(t)$ in a velocity field $v(x, t)$, so that the dynamics is simple,

$$\frac{dx_i}{dt} = v(x_i, t). \quad (1)$$

We assume that the velocity field $v(x, t)$ is a random function of time so that each particle displays a random one-dimensional motion. For the differential equation (1) to be well-posed, the field $v(x, t)$ should be smooth enough in x (at least Lipschitz continuous).

One typically associates advection with a transport by moving fluid, and fluids are in most cases nearly incompressible, so that in one dimension the velocity is constant. However, the velocity field on the surface of incompressible fluid can be any function of coordinate and time. Thus, the one-dimensional setup directly applies to particles floating on the surface of a two-dimensional turbulent flow. This flow can be random surface waves (see Ref. [7] for experiments involving particles’ advection in two-dimensional surface waves, and Ref. [8] for the recent realization of turbulent one-dimensional surface waves). Another possible source of one-dimensional random advection is two-dimensional turbulent convection (e.g., in a Hele-Shaw cell) with an open upper surface, on which the floating particles move.

The main macroscopic effect is the merging/clustering/coalescence (we use these terms as synonyms below) of particles. Indeed, if the coordinates of two particles coincide at $t = 0$, $x_i(0) = x_j(0)$, then their trajectories are identical at any later time, i.e., $x_i(t) \equiv x_j(t) = X(t) \quad \forall t > 0$, with $\dot{X} = v(X, t)$ and $X(0) = x_{i,j}(0)$. A cluster of particles with identical positions is, therefore, a solution of Eq. (1). A second and equally important remark is that such a solution is stable in the sense that neighboring particles get effectively “attracted” to each other to form a cluster. To see this, suppose that the field

$v(x, t)$ is a smooth enough function of x , so that one can linearize (1) around a reference trajectory of a cluster $X(t)$, to obtain for a small perturbation Δx

$$\frac{d}{dt} \Delta x = \Delta x \frac{\partial}{\partial x} v(X(t), t). \quad (2)$$

This linear equation with a random function of time $v(X(t), t)$ defines the Lyapunov exponent

$$\lambda = \left\langle \frac{\partial}{\partial x} v(X(t), t) \right\rangle_t \quad (3)$$

so that asymptotically in time, $\Delta x(t) \propto \exp[\lambda t]$.

The main observation is that in one-dimensional continuous dynamics, the Lyapunov exponent cannot be positive because the phase volume for a statistically stationary regime cannot grow indefinitely. Furthermore, it is improbable for random fields that the Lyapunov exponent vanishes. Indeed, in nonrandom one-dimensional dynamics, the Lyapunov exponent can be either negative (a sink) or zero (e.g., a steady periodic motion over a periodic space profile). Randomness “mixes” these two situations, thus leading to a negative Lyapunov exponent. For a negative Lyapunov exponent, $\Delta x \rightarrow 0$ as $t \rightarrow \infty$. This means that neighboring particles glue together (coalesce), and in a finite system a stable cluster forms at long enough times. Since *all* the particles have the same trajectory there, we will refer to it as the *maximal cluster*. Also, since the cluster will perform a random motion, we will, for definiteness, refer to this motion as *macrodiffusion*.

We note here that coalescence to a maximal cluster also occurs in more general situations, provided the maximal Lyapunov exponent is negative. For example, such a situation is possible for two-dimensional advection as well, although in this case there are two Lyapunov exponents, so the maximal one may become positive and the cluster will be destroyed. One class of problems where a maximal cluster appears is irreversible aggregation, where a large number of small particles coalesce over time with no possibility of breaking up; see Ref. [9] and the literature therein. On the other hand, in the context of noise-driven dynamical systems the effect of the formation of the maximal cluster has been termed *synchronization by common noise*, and it was first described in Refs. [10,11], where an ensemble of identical systems (i.e., an ensemble of different initial conditions) driven by the same realization of noise was analyzed. In the mathematical literature, equations of type (1) are called random dynamical systems, and a maximal cluster state as described above represents a point random attractor in such a system [12]. The effect of synchronization by common noise also appears in neuroscience (there it is called reliability [13]), and in other fields [14,15]. If the maximal Lyapunov exponent becomes positive (which is possible starting from dimension 2), a point attractor undergoes a transition to a fractal one [16,17]. In the context of passive scalar advection theory, such a transition, which occurs as the compressibility of the underlying flow increases, was discussed in [18].

The nature of the macrodiffusion (i.e., whether it is normal or anomalous) depends on the actual statistical properties of the field $v(x, t)$ (cf. [19]). In the examples considered below, we will limit ourselves to the case in which spatial and tempo-

ral correlations of the velocity field decay rapidly, so that the macrodiffusion will be normal.

We stress that the arguments about attracting clustered states are valid for a large but finite system. This will be the case we consider in this paper, where we also will explore scaling relations as the size of the system goes to infinity.

Although a clustered state is an attractor in the random advection dynamics (1), there can be several such attractors in degenerate situations. Indeed, if, e.g., the velocity field is odd in space, $v(-x, t) = -v(x, t)$, then $v(0, t) = 0$ and the particles starting in positive $x > 0$ and negative $x < 0$ domains never meet and never merge, so there are at least two attractors here. Below, we assume that such a degenerate situation does not occur, and we have one ergodic component: all the initially distributed particles evolve under (1) to one single maximal cluster.

The above concept of macrodiffusion should be juxtaposed with a familiar Brownian motion, as given by the Langevin equations

$$\frac{dx_i}{dt} = \sigma \xi_i(t), \quad (4)$$

where the microscopic noises $\xi_i(t)$ are zero-average, independent (i.e., different for different particles) Gaussian and white noises with $\langle \xi_i(t) \rangle = 0$, $\langle \xi_i(t) \xi_j(t') \rangle = 2\delta_{ij} \delta(t - t')$. This noise leads to a diffusive spreading $\sim \sigma^2 t$ of particles in the ensemble. We call this effect *microdiffusion* for a clear distinction with the above.

Our main goal in this paper is to contribute to an understanding of the behavior of an ensemble of particles, where both macro- and microdiffusion in a given random velocity field are present; namely, we combine (1) and (4) into an equation

$$\frac{dx_i}{dt} = v(x_i, t) + \sigma \xi_i(t). \quad (5)$$

We illustrate different regimes in the dynamics of (5) in Fig. 1.

Equation (5) can be considered as a Langevin equation so that the evolution of the probability density $w(x, t)$ of an ensemble of particles obeys the Fokker-Planck equation

$$\frac{\partial}{\partial t} w + \frac{\partial}{\partial x} (v(x, t)w) = \sigma^2 \frac{\partial^2 w}{\partial x^2}. \quad (6)$$

We stress that this equation includes averaging over the microscopic noise terms $\xi(t)$ but still contains the random function $v(x, t)$, which is common for all the particles. Thus, formally this equation is a stochastic partial differential equation.

Our main interest is in the statistical properties of the density $w(x, t)$. As argued above, in the absence of microdiffusion, $\sigma = 0$, the asymptotic state is a point attractor (cluster) which moves randomly: $w(x, t) = \delta(x - X(t))$. This singular solution becomes “smeared” by a finite microdiffusion $\sigma > 0$. However, the details of this continuous random field $w(x, t)$ are not clear *a priori*, and the goal of this paper is to contribute to understanding the statistical properties of the distribution density w .

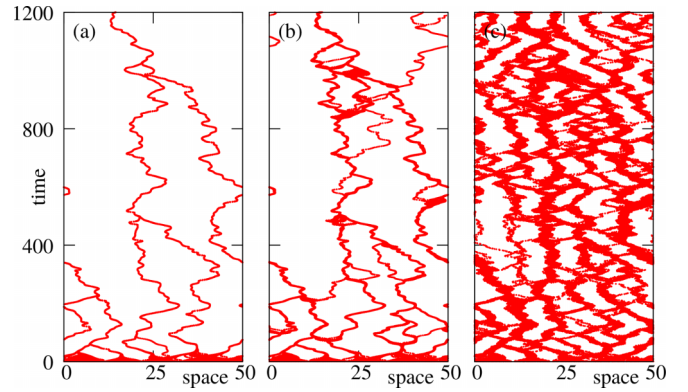


FIG. 1. Dynamics of a set of 200 particles, initially uniformly distributed, according to Eq. (5) for different levels of microdiffusion σ , for the same realization of random field $v(x, t)$ (this field is taken as a chaotic solution of the Kuramoto-Sivashinsky equation; cf. [19]). (a) Microdiffusion-free case $\sigma = 0$; here one observes a perfect formation of the maximal cluster. (b) Small noise $\sigma = 0.005$; here some particles due to noise split from the largest cluster, which, however, contains most of them. (c) Large noise $\sigma = 0.3$; here the distribution of particles is nonuniform, but there are no dominating clusters.

III. LATTICE MODELS

It is computationally rather costly to simulate Eq. (6) on a large domain and for small σ . Furthermore, the results are expected to depend drastically on the statistical characteristics of the underlying velocity field $v(x, t)$. In the literature, one has taken for this field turbulent solutions of the deterministic Kuramoto-Sivashinsky equation [19,20] as in Fig. 1. Another approach is to interpret the advective motion as sliding along a one-dimensional surface $v(x, t) = \partial_x h(x, t)$, and to use one of the popular stochastic partial differential equations for the dynamics of this surface $h(x, t)$, e.g., the Edwards-Wilkinson equation [21] or the Kardar-Parisi-Zhang equation [22]; see Refs. [23–28]. Although there are statistical models for one-dimensional wave turbulence [29], including the deterministic fractional partial differential equation (PDE) by Majda, McLaughlin, and Tabak [30], we are not aware of any study of advection in such models.

A convenient approach to finding scaling properties of random advection is to explore proper lattice models. In a lattice model, the field is discrete in space, and therefore one cannot perform a continuous stability analysis of a cluster state like in Eq. (2) above. Indeed, if one takes the continuous-in-space model (1), then a natural assumption is that the velocity fields at large distances are independent, but at small distances [at which the linearization (2) is valid] it is smooth. Thus, if one takes two particles at a large initial distance, they first diffuse independently, and only when they are close enough to each other do they merge according to the Lyapunov exponent (3). A lattice model can imitate the first stage of independent diffusion but replaces the second stage of exponential convergence with an abrupt coalescence. Furthermore, the lattice models below are formulated in a discrete time. In these models, one defines a conserved “mass field” $u_k(t)$, where k is the lattice site and t is discrete time. This field should be interpreted as a discretized density $w(x, t)$ of advected particles from

Eq. (6). As is clear from the discussion of existing continuous models above, one can construct lattice models with different statistical characteristics. Below we will focus on “maximally random” lattice models, with vanishing correlations of the effective “velocity field” in space and time. The motion of a single particle in such models is pure diffusion, in contradistinction to a superdiffusion due to time-correlation of the velocity in the cases mentioned above [19,20,26].

A. Generic two-site models

We start with a rather generic setup and then focus on two particular lattice models that will be considered below. We assume that the models for a continuous field on a lattice are formulated as follows:

(i) A pair of neighboring (to ensure locality) sites, $(k, k + 1)$, is chosen randomly.

(ii) The fields at these sites, u_k, u_{k+1} , are redistributed according to a deterministic (parameters fixed) or stochastic (parameters chosen from a distribution) linear rule,

$$u'_k = (1 - a)u_k + bu_{k+1}, \quad (7)$$

$$u'_{k+1} = au_k + (1 - b)u_{k+1}, \quad (8)$$

where the primes indicate the masses after a move, and where we have implemented mass conservation.

Therefore, the rule is generically described by a stochastic matrix depending on two parameters $0 \leq a, b \leq 1$:

$$\mathbf{A}(a, b) = \begin{pmatrix} 1 - a & b \\ a & 1 - b \end{pmatrix}.$$

If $a \neq b$, the distribution is asymmetric. Thus, for fixed $a \neq b$, one applies matrices $\mathbf{A}(a, b)$ and $\mathbf{A}(b, a)$ with probabilities $1/2$. Such a symmetrization might not be needed if a, b are chosen as random variables. We note that the parameters $k, k + 1$ and matrix $\mathbf{A}(a, b)$ do not depend on the field u , thus the particles are *passive*. For a lattice model of an *active* particle sliding over a surface, which is influenced by the particle position, see [31].

In terms of these parameters, different models from the literature (see Fig. 2) can be described as follows:

(i) *The Kang-Redner (KR) model* [32] (see a detailed description in Sec. III B below) corresponds to $a = 1, b = 0$: all the mass of a random site i is transferred to a random neighbor $i \pm 1$.

(ii) *The Takayasu-Taguchi (TT) model* [33] (see a detailed description in Sec. III C below) corresponds to $a = 1 - \epsilon, b = 0$: the fraction a of the mass of a random site i is transferred to a random neighbor $i \pm 1$.

(iii) *The Kipni-Marchioro-Presutti (KMP) model* [34] (see discussion in Sec. VIII) corresponds to $a = 1 - b = \xi$, where ξ is uniformly distributed $0 \leq \xi \leq 1$: the total mass of a random pair of neighboring sites is randomly redistributed between them.

(iv) *The Rajesh-Majumdar (RM) model* [35] (see discussion in Sec. VIII) in the limiting case of a sequential update is a random version of the TT model $a = \xi, b = 0$, where ξ is uniformly distributed, $0 \leq \xi \leq 1$.

(v) *The deterministic KMP (det-KMP) model* (it looks like this model has not been considered before) corresponds to $a =$

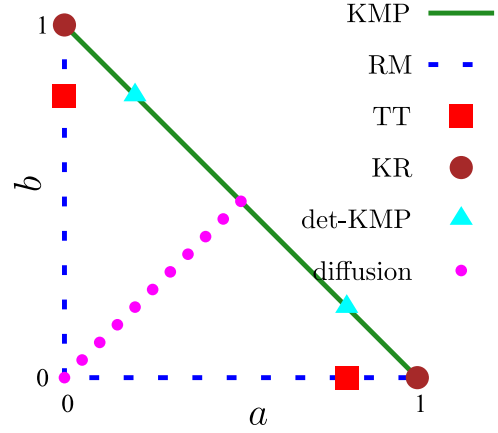


FIG. 2. Different models in terms of parameters (a, b) . Cases TT, KR, and det-KMP with fixed parameters (except for diffusion) are shown with markers (for definiteness, we take $\epsilon = 0.8$); cases KMP and RM, where parameters are random, are shown with green solid and blue dashed lines, respectively, upon which the values of these parameters lie. The case of diffusion is shown with a magenta dotted line.

$\epsilon, b = 1 - \epsilon$: a certain portion of the total mass of a random pair of neighboring sites is distributed between them in a fixed proportion.

(vi) *Diffusion*. This is a situation when $a = b$ (either fixed or random): a random site gains (or loses) a fraction of the mass difference between it and a neighboring site.

In this paper, we focus on the KR and TT lattice models, and we discuss the relation to KPM, RM, det-KPM, and some models based on the particle dynamics in Sec. VIII.

B. Kang-Redner model

This setup is attributed to Smoluchowski; it describes coalescence without microdiffusion (i.e., at $\sigma = 0$). We outline it following Ref. [32] (where this model is also discussed in dimensions higher than 1). In this KR model, the field u_k is fully discrete: on each site of a discrete, regular one-dimensional lattice, the mass is an integer number of “particles,” $u_k = 0, 1, 2, \dots$. Such masses macrodiffuse with a constant diffusion constant, according to the following sequential update: at each time step, a site k is chosen at random, along with the direction of motion (\pm , also chosen at random). Then the mass migrates from site k to the neighboring site:

$$\begin{aligned} u_k(t + 1) &= 0, \\ u_{k\pm 1}(t + 1) &= u_{k\pm 1}(t) + u_k(t). \end{aligned} \quad (9)$$

This model is sometimes called the $A_i + A_j \rightarrow A_{i+j}$ kinetic reaction [9]. Clearly, on a finite lattice of size L , the distribution of masses converges to a state where all the particles occupy the same lattice site, and this maximal cluster performs a random walk.

The relaxation dynamics towards such a final state is characterized by the temporal evolution of the probability $c_m(t)$ to have a cluster of $m > 0$ particles. In one dimension and in the infinite domain, the authors of [32] provide the following

scaling relation for $c_m(t)$:

$$c_m(t) \sim \frac{m}{t^{3/2}} f\left(\frac{m}{t^{1/2}}\right), \quad m > 0,$$

where $f(x) \rightarrow \begin{cases} 1, & x \ll 1, \\ 0 \text{ (rapidly)}, & x \gg 1. \end{cases}$ (10)

A similar result, $c_m(t) \sim \frac{m}{t^{3/2}}$, valid for $m \ll t^{1/2}$ is derived in [36]. We notice here that one can also formulate the KR model for masses that are not integers, but any non-negative real numbers (as is assumed, e.g., in the Takayasu-Taguchi model below). The phenomenology is the same: over the course of time, masses coalesce, and in a finite system, eventually, one moving maximal cluster contains all the initial mass. However, in this case, one has to generalize the discrete distribution $c_m(t)$ into a continuous one; thus, we stick to the original Kang-Redner formulation for discrete particles.

C. Takayasu-Taguchi model

In this work, we will focus on another microscopic model, first introduced by Takayasu and Taguchi in Ref. [33]. It is defined for a continuous lattice field $u_k(t)$ on sites $k = 1, \dots, L$ (with periodic boundary conditions) and discrete time, $t = 0, 1, 2, \dots$. The dynamical rule is very similar to that in the KR model. For a randomly chosen site k and a randomly chosen “direction” \pm , the field is updated as

$$u_k(t+1) = \epsilon u_k(t),$$

$$u_{k\pm 1}(t+1) = u_{k\pm 1}(t) + (1 - \epsilon)u_k(t). \quad (11)$$

The parameter $0 \leq \epsilon < 1$ gauges the strength of field transport, because a fraction $(1 - \epsilon)$ of the mass u_k is transported to a neighboring site and added to $u_{k\pm 1}$ [37] (the case $\epsilon = 1$ is trivial because there is no dynamics). By construction, the dynamics conserves the total mass, $\sum_k u_k$.

The TT dynamics entails both macro- and microdiffusion, their relative strengths being controlled by the parameter ϵ . This follows from the following two interesting limits.

(i) For $\epsilon \rightarrow 1$ the advection is weak, so the microdiffusion is relatively strong. In this case, at each step, a small portion of the field at a randomly chosen site is transferred left or right [38].

(ii) On the other hand, the case $\epsilon = 0$ is one without microdiffusion but with pure random advection. It is also termed irreversible aggregation in Ref. [33]. Here, the fields at neighboring sites merge (coalesce), but no further splitting is possible. In fact, one can easily see that for $\epsilon = 0$ the TT model (11) is essentially the same as the KR model (9), the only difference being the allowed set of values of u_k : in the KR model these values are integers, while in the TT model they are non-negative real numbers. However, this difference appears to be irrelevant for large systems and for large times when clusters with large occupations emerge.

It should also be mentioned that some variants of the TT model, including external injection, have been considered in Refs. [39,40].

D. Takayasu-Taguchi model with global coupling

In the following, we will also consider a variant of the TT model with *global* interaction. By this we mean that the

exchange does not occur between the neighbors but rather between two independently randomly chosen sites k, m . Evolution follows the same rule,

$$u_k(t+1) = \epsilon u_k(t),$$

$$u_m(t+1) = u_m(t) + (1 - \epsilon)u_k(t). \quad (12)$$

Remarkably, this model is exactly the multiplicative random exchange model, introduced in [41] to describe wealth redistribution in a population. In general, wealth redistribution models share some properties, such as conservation of the total mass, with the random advection models above, but they are typically formulated with discrete agents not on a lattice (so that there is no spatial organization and, correspondingly, no locality) but with global coupling; see [42–44].

E. The TT model as an iterated function system

The TT model has a remarkable mathematical interpretation as an iterated function system (IFS) with probabilities [45]. Indeed, each advection event in (11) is a linear contracting transformation of the vector $\{u_k\}$, and there are altogether $2L$ such transformations (L sites multiplied by two possible transport directions). Thus the probability for one particular transformation is $(2L)^{-1}$. Evolution is a composition of these transformations and fulfills the definition of an IFS (see Chap. IX of Ref. [45]). Typically, IFSs are used to produce fractal measures. We show in Appendix A that, indeed, one gets a fractal distribution (although not for all values of ϵ) in small lattices with $L = 2, 3$. In this paper, we are mainly interested in the case of large systems $L \gg 1$; thus, we will focus not on the fractal properties of the field $\{u_k\}$ (which are nevertheless hardly accessible in numerics), but on the statistical properties.

IV. STATISTICAL PROPERTIES OF THE KR MODEL ON A FINITE LATTICE

In this section, we report on the scaling properties of the coalescence process on finite lattices without microdiffusion. This corresponds to the KR model (9) or to the TT model (11) with $\epsilon = 0$. In fact, this section aims to extend the scaling relation (10) (valid for an infinite system) to the case of lattices of finite size L .

In numerical simulations, we start with a uniform initial state $u_k(0) = 1, k = 1, \dots, L$. Because in this section masses $u_k(t)$ are integers, we refer to these quantities as “number of particles” at site k , or a “cluster of size u_k .” As expected from the general discussion in Sec. II, the final state after all the particles merge to a single site (i.e., they form the maximal cluster of size L) is $u_k(t) = L\delta_{kj}$, where $j(t)$ is the random position of the maximal cluster. The characteristic diffusion time of a particle in the lattice of length L is $T_d(L) = L^2$. [Because in the models (9) and (11) the update is sequential, the time here and below is measured in units of L to make it possible for every site to move in one effective time unit.] We thus expect that $T_d(L)$ is the time required for the formation of the maximal cluster. We now discuss the dynamics in the two relevant regimes.

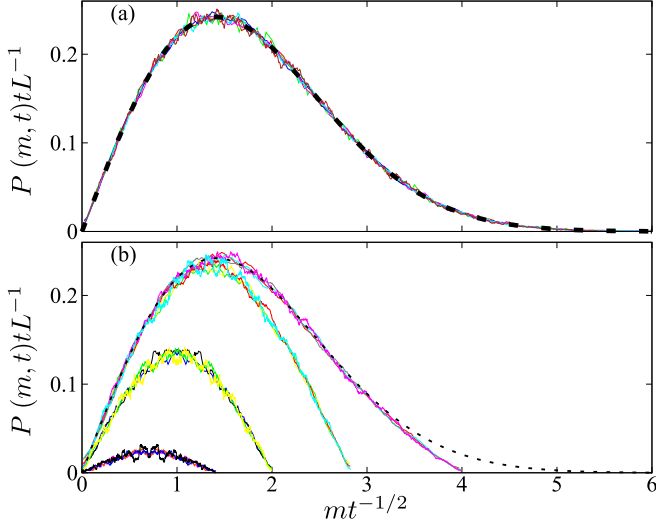


FIG. 3. Scaled probability distributions for the KR model at different times and lattice sizes. (a) Short times, $t \ll T_d$. Data for different L and different times: there are six nearly overlapping curves for $L = 256$, $t = 512$; $L = 256$, $t = 1024$; $L = 512$, $t = 2048$; $L = 512$, $t = 4096$; $L = 1024$, $t = 16384$; $L = 1024$, $t = 32768$. The “guess” (14) $\mathcal{F}(m/t^{1/2})$ (black dashed line) seems also to be very good. In all runs, averaging over 32 768 realizations is performed. Additionally, the curves for $L = 512$ and 1024 are locally smoothed by a running window (otherwise, fluctuations are relatively large). (b) The same but for large times. For four lattice lengths $L = 128, 256, 512, 1024$ the instants of time correspond to $t = T_d/16, T_d/8, T_d/4, T_d/2$ (nearly overlapping curves from top to bottom), with $T_d = L^2$. The curve $\mathcal{F}(x)$ is also shown as the dashed line for comparison on this panel.

A. Short times: $t \ll T_d$

On this timescale, the scaling properties of the infinitely large system should hold. Indeed, KR give a scaling relation (10) (on an infinite lattice) for the average (over realizations of random advection) number of sites $P(m, t)$ possessing a cluster of mass $m > 0$ at time t . We expect this relation to hold on a finite lattice for small times. To compare results for different lattice sizes L , it is convenient to modify the scaling of (10) by multiplying by L (to pass from a probability to an average number of sites) and incorporating a factor $m/t^{1/2}$ in the scaling function, so that

$$P(m, t) = t^{-1} L F_1(m t^{-1/2}). \quad (13)$$

Because $L = \sum_m m P(m, t) \approx \int_0^\infty dm m P(m, t)$, we conclude that normalization of $F_1(x)$ is independent of L :

$$\int_0^\infty dx x F_1(x) = 1.$$

It is noteworthy that $\sum_m P(m, t)$ (the total number of nonempty sites) is not normalized to L . In fact, $\sum_m P(m, t) \simeq L/\sqrt{t}$, which is the equivalent of the relation $\sum_m c_m(t) \simeq t^{-1/2}$ given by Kang and Redner [32].

In Fig. 3(a), we show the simulations for $L = 256, 512, 1024$. We observe that (i) the data for different L and t collapse nearly perfectly, and (ii) a guess (black

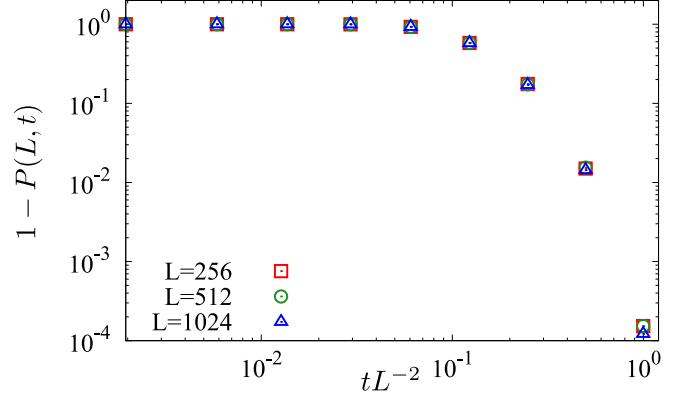


FIG. 4. Probability for the maximal cluster with occupation L to occur, Eq. (16), as a function of the scaled time t/L^2 , for different $L = 256, 512, 1024$.

dashed line) in the form of a simple analytical expression,

$$\mathcal{F}(x) = \frac{x}{\sqrt{4\pi}} \exp\left[-\left(\frac{x}{2}\right)^2\right], \quad (14)$$

provides a very close fit of the observed data.

B. Large times: $t \lesssim T_d$

For large times $t \approx T_d$, when the probability for the maximal cluster to exist, $P(L, t)$, is not negligible, the distribution $P(0 < m < L, t)$ deviates from that for infinite lattices, as shown in Fig. 3(b). Nevertheless, the distributions overlap for the same values of t/T_d . This observation suggests a finite-size generalization of scaling (13) of the form

$$P(m, t) = t^{-1} L F_2(m t^{-1/2}, m/L) + \delta_{m,L} P(L, t), \quad (15)$$

where in F_2 , one has $m < L$ (in other words, this function describes all clusters that are less than the maximal one) and δ_{ij} is the Kronecker delta. The separation into two parts, the maximal cluster and the rest, allows us to use a continuous approximation for F_2 . This scaling function now depends on two arguments: $F_2(x, y)$, $x = m/t^{1/2}$, $y = m/L$, and it must satisfy the following properties: (i) As $L \rightarrow \infty$, the scaling (13) must hold, thus $F_2(x, 0) = F_1(x)$; (ii) there is no cluster with a size larger than L (and the maximal cluster of size L is not included to the distribution), thus $F_2(x, y \geq 1) = 0$ [46]. From the normalization $L = \sum_m m P(m, t)$, the expected scaling for the probability of the maximal cluster follows directly:

$$P(L, t) = 1 - L^{-1} \int_0^\infty dm m t^{-1} L F_2\left(\frac{m}{t^{1/2}}, \frac{m}{L}\right) = s(t/L^2). \quad (16)$$

This relation is verified in Fig. 4.

We check the validity of Eq. (15) in Fig. 5. Here, we plot the distributions, rescaled according to Eq. (15), for several different fixed values of $x = m/t^{1/2}$, namely we plot $G(m, t) = t L^{-1} P(m, t) / \mathcal{F}(m/t^{1/2})$ versus $y = m/L$. For each x considered, one can see a nice overlap of data obtained for several different sizes $L = 128, 256, 512$, supporting the ansatz (15). As expected, G tends to 1 for $x \rightarrow 0$ and vanishes for $x \rightarrow 1$. Another confirmation of scaling (15) is the bottom panel of Fig. 3.

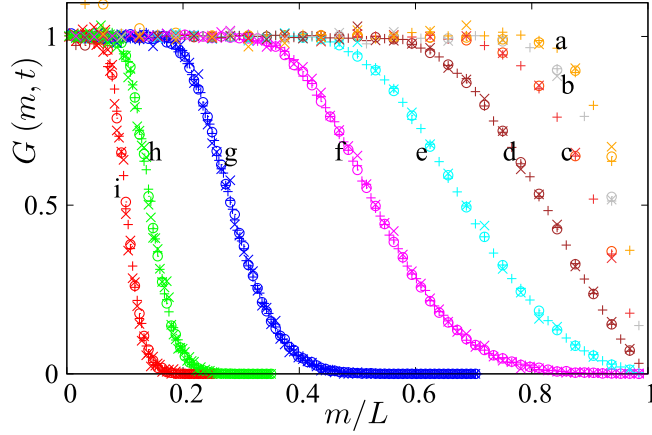


FIG. 5. Plot of the rescaled distributions $G(m, t) = tL^{-1}P(m, t)/F(mt^{-1/2})$ at different values of $mt^{-1/2}$ [different colors and gray levels: from top right to bottom left, $mt^{-1/2} = 4$ (yellow, set a), $mt^{-1/2} = 3.46$ (grey, set b), $mt^{-1/2} = 2.83$ (dark red, set c), $mt^{-1/2} = 2$ (brown, set d), $mt^{-1/2} = 1.41$ (cyan, set e), $mt^{-1/2} = 1$ (magenta, set f), $mt^{-1/2} = 0.5$ (blue, set g), $mt^{-1/2} = 0.25$ (green, set f), and $mt^{-1/2} = 0.177$ (red, set i) as a function of the rescaled variable $y = m/L$, for $L = 128$ (open circles), $L = 256$ (pluses), and $L = 512$ (crosses).

C. Roughening properties in the KR model

Let us now describe the mass distribution $u_k(t)$ interpreting it as an “interface” profile, whose width $W(L, t, \epsilon)$ is defined as usual in the following way:

$$W^2 = \langle (u - \langle u \rangle)^2 \rangle, \quad (17)$$

where $\langle \cdot \rangle$ is both a spatial and a statistical average. Since this quantity will also be used later on, we made explicit the dependence on the parameter ϵ , which distinguishes the TT model from the KR model (the models are equivalent for $\epsilon = 0$).

Since the field is conserved, with our choice of the initial conditions $\langle u \rangle = 1$ always. Following the Family-Vicsek scaling approach [47], we can write

$$W(L, t, 0) \sim L^\chi g\left(\frac{t}{L^z}\right), \quad (18)$$

where $g(\xi)$ is a suitable scaling function with $g(\xi) \sim \xi^\beta$ for $\xi \ll 1$ and $g(\xi) \sim 1$ for $\xi \gg 1$, so that $W(L, t, 0) \sim t^\beta$ at short times ($t \ll L^z$, growth regime) and $W(L, t, 0) \sim L^\chi$ at long times ($t \gg L^z$, saturated regime). The growth exponent β , the roughness exponent χ , and the dynamical exponent z are related by $\chi = \beta z$.

In the specific case that we are considering in this section (the KR model), it is clear that the crossover time between the two regimes is given by the diffusive time $T_d = L^2$, so that $z = 2$. At short times we can make use of the scaling relation (13) for the probability to have a height k :

$$\begin{aligned} L^{-1}P(m, t) &= \begin{cases} t^{-1}F_1(mt^{-1/2}), & m > 0, \\ 1 - \int_0^\infty t^{-1}F_1(mt^{-1/2})dm = 1 - \frac{1}{\sqrt{\pi t}}, & m = 0 \end{cases} \end{aligned}$$

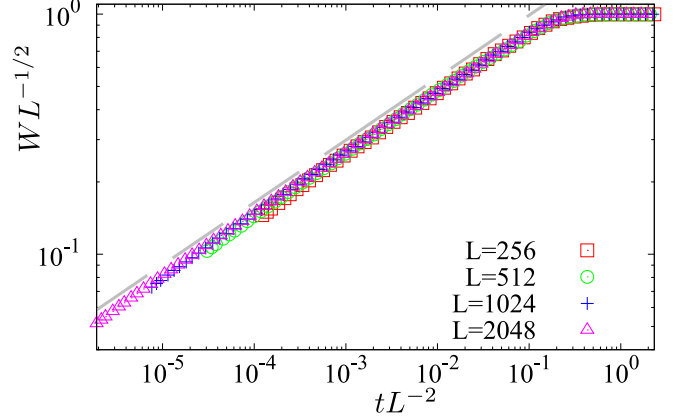


FIG. 6. Evolution of the width $W(L, t, 0)$ in the KR model for different L in the rescaled coordinates. The gray dashed line has slope 0.26, close to the exponent β predicted by Eq. (19). Data collapse on the scaling function $g(t/L^2)$.

[in the last expression, we calculated the integral using function (14)]. Thus the width can be computed explicitly using expression (14) for F_1 :

$$W^2 = \int_0^\infty L^{-1}P(m, t)(m-1)^2 dm = \frac{4t^{1/2}}{\sqrt{\pi}} + 3.$$

Because the scaling holds for $t \gg 1$, we can assume

$$W \approx 2\pi^{-1/4} t^{1/4},$$

which yields the exponent $\beta = 1/4$ and therefore $\chi = 1/2$. Altogether, we come to the scaling relation

$$W(L, t, 0) = L^{1/2} g\left(\frac{t}{L^2}\right). \quad (19)$$

This theoretical prediction is successfully checked in Fig. 6. The scaling function $g(t/L^2)$ could be formally expressed in terms of the scaling function $F_2(x, y)$, but this would be a futile exercise, especially because we do not know the analytic form of $F_2(x, y)$ [while we do have a very good expression for $F_1(x)$].

At first glance, one may argue that $\beta = 1/4$ and $\chi = 1/2$ are the Edwards-Wilkinson (EW) [21] roughening exponents in $d = 1$. However, this is just a coincidence because, at variance with EW, the distributions are *not* Gaussian. This should be traced back to the fact that, in the present model, the total mass is conserved, while in EW it is not (see, however, a discussion of the conserved EW in Sec. VIB below).

In this respect, mass conservation might inspire one to compare the model under consideration with the conserved KPZ equation [48–50]. In one dimension, it reads

$$\begin{aligned} \frac{\partial \phi}{\partial t} &= -\nabla^2[\kappa \nabla^2 \phi + \lambda |\nabla \phi|^2] + \eta(x, t), \\ \langle \eta \rangle &= 0, \quad \langle \eta(x, t) \eta(x', t') \rangle = -2D \nabla^2 \delta(x - x') \delta(t - t'), \end{aligned} \quad (20)$$

and fulfills mass conservation $\int \phi(x, t) dx = \text{const}$. However, the dynamic exponents characterizing roughening in this equation are $z = 11/3$, $\beta = 1/11$, and $\chi = 1/3$ [48], which

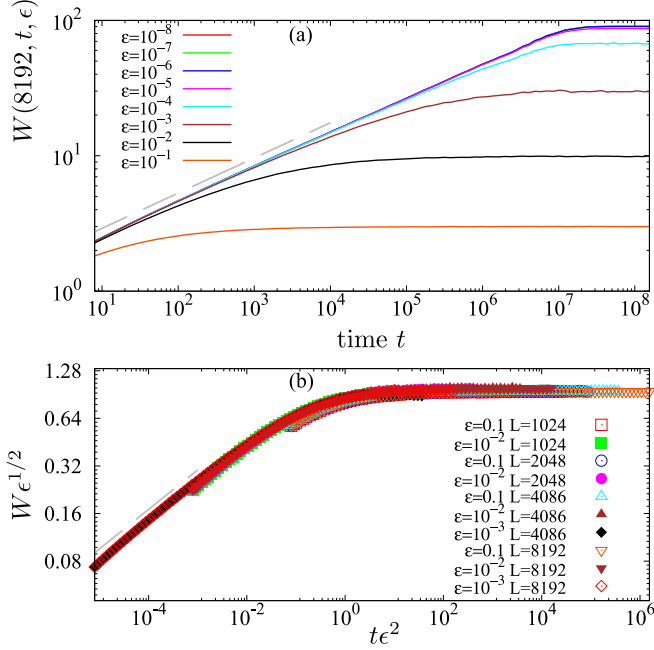


FIG. 7. (a) Field widths $W(L, t, \epsilon)$ as a function of time for different ϵ (increasing from top to bottom) and $L = 8192$. The dashed line has a slope of 0.26, which is close to the theoretical value 0.25 derived for $\epsilon = 0$. (b) Widths of the field in dependence on time for different ϵ , L in scaled coordinates. The dashed line has a slope of 0.25.

are distinctly different from ours. This is not surprising because there are two basic differences between (6) and (20): (i) In (20) the noise is additive, and in (6) it is multiplicative; (ii) the CKPZ equation is nonlinear while the random advection equation (6) is linear.

V. EVOLUTION TO A STATIONARY STATE IN THE TT MODEL: OVERALL PICTURE

Let us now turn to the case in which parameter ϵ in (11) is nonzero. In other words, both macrodiffusion and microdiffusion are present. We first performed the same roughening experiment as above but with the TT model. The results for different values of L and ϵ are presented in Fig. 7. Both panels clearly indicate that, for a finite system, a statistically stationary regime is established at long times. However, the evolution of the width crucially depends on parameter values ϵ , L . In panel (a) of Fig. 7, where we fix $L = 8192$, one can clearly see that the values of ϵ can be separated into two ranges. For $\epsilon \lesssim 10^{-5}$, there is no significant ϵ -dependence in $W(L, t, \epsilon)$; the curves follow the roughening in the KR model (19). In contradistinction, for $\epsilon \gtrsim 10^{-4}$, the dependence of $W(L, t, \epsilon)$ on ϵ is significant, and the saturated width $W(L, \infty, \epsilon)$ decreases with ϵ . Therefore, for large values of ϵ , we plot the data in another scaling that includes ϵ in Fig. 7(b). Now the data for different L overlap, which indicates that the “roughening” is not L -dependent. In other words, in this regime there is no true roughening because the saturated width is system-size-independent (but depends on the parameter ϵ).

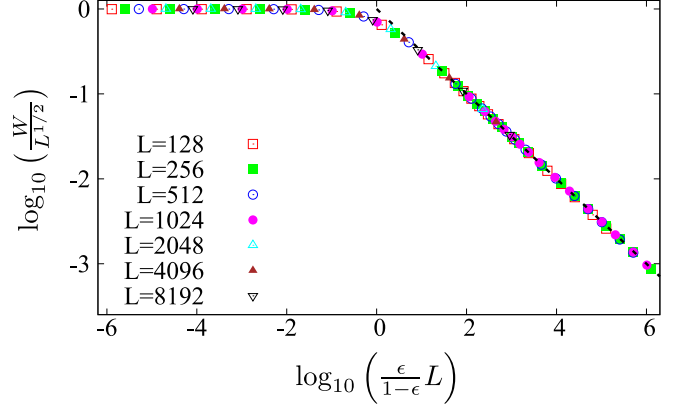


FIG. 8. Asymptotic ($t \rightarrow \infty$) roughness $W(L, \infty, \epsilon)$ as a function of the system size L and of the parameter ϵ . Data collapse shows that $W(L, \infty, \epsilon) = L^{1/2}f(\epsilon L/(1 - \epsilon))$, where the scaling function $f(u)$ has the limiting behavior $f(u) = 1$ for $u \ll 1$ and $f(u) = u^{-1/2}$ for $u \gg 1$. The dashed line has a slope of $-1/2$.

A clean way to analyze the separate effects of the system size L and of the parameter ϵ is to focus on the asymptotic, time-independent width $W(L, \infty, \epsilon)$. This is done in Fig. 8, where we plot $W(L, \infty, \epsilon)/L^{1/2}$ versus $\epsilon L/(1 - \epsilon)$. The data of Fig. 8 cover a wide range of values of L and ϵ and clearly indicate the existence of two types of stationary states:

(i) *Macrodiffusion-dominated regime*. This regime corresponds to the leftmost part of the graph where the scaled width $WL^{-1/2}$ does not depend on ϵ . Here the width scales as $W \sim L^{1/2}$ like in the KR model at $\epsilon = 0$. Nevertheless, the state here is nontrivial and will be discussed in detail in Sec. VII below.

(ii) *Microdiffusion-dominated regime*. This regime corresponds to the rightmost part of the curves in Fig. 8, where the scaling $WL^{-1/2} \sim (\frac{\epsilon}{1-\epsilon}L)^{-1/2}$ holds. This means that here the width does not depend on the system size L : $W \sim (\frac{\epsilon}{1-\epsilon})^{-1/2}$. We discuss this regime in Sec. VI below.

The crossover between two regimes occurs at $(\frac{\epsilon}{1-\epsilon}L) \approx 1$, i.e., at $\epsilon L \approx 1$. We remark that the microdiffusion-dominated regime is attained when $\epsilon \gg 1/L$ but also for $\epsilon \rightarrow 1$ and rather small L . A final comment about simulations is in order here. While it is relatively easy to vary parameter ϵ in a wide range, for the length L we can hardly significantly increase the range beyond several thousand.

Below in Secs. VI and VII, we will focus on the detailed analysis of stationary regimes for microdiffusion- and macrodiffusion-dominated regimes, respectively.

VI. STRONG MICRODIFFUSION $\epsilon > L^{-1}$

The discussion above shows that the system length is irrelevant here.

A. Mean-field theory

We start with the mean-field theory, where spatial correlations are neglected (our approach is similar to that of Ref. [33] but it does not coincide with it). With probability 1/2, each site either delivers part of its field to a neighbor or it receives a part of the neighbor’s field. Thus, the updating rule for a

field at a given site reads $u \rightarrow \bar{u}$,

$$\bar{u} = \begin{cases} \epsilon u & \text{Prob } 1/2, \\ u + (1 - \epsilon)v & \text{Prob } 1/2, \end{cases} \quad (21)$$

where v is the field of the neighbor. In the mean-field approach, we assume statistical independence of u and v , which have the same distribution. This allows us to express the evolution of the density through a Perron-Frobenius operator (w and \bar{w} denote densities at the subsequent time steps),

$$\begin{aligned} \bar{w}(x) &= \langle \delta(x - \bar{u}) \rangle = \frac{1}{2} \int_0^\infty du w(u) \delta(x - \epsilon u) \\ &+ \frac{1}{2} \iint_0^\infty du dv w(u)w(v) \delta(x - u - (1 - \epsilon)v) \\ &= \frac{1}{2\epsilon} w\left(\frac{x}{\epsilon}\right) + \frac{1}{2} \int_0^{x(1-\epsilon)^{-1}} dv w(x - (1 - \epsilon)v)w(v). \end{aligned} \quad (22)$$

Unfortunately, we cannot solve this equation analytically, except for the case $\epsilon = 1/2$, for which one can easily check that the solution is an exponential distribution $w(u) = \exp(-u)$. Indeed, in this case the calculation of the right-hand side of (22) is straightforward:

$$\begin{aligned} w(2x) + \frac{1}{2} \int_0^{2x} dv e^{-x+v/2} e^{-v} \\ = e^{-2x} + \frac{e^{-x}}{2} \int_0^{2x} e^{-v/2} dv = e^{-x}. \end{aligned}$$

It is possible, however, to express, for arbitrary ϵ , all the moments $M_n = \langle u^n \rangle$ explicitly in a recursive manner. Indeed, it follows directly from (21) that $M_n = \frac{1}{2} \langle (\epsilon u)^n \rangle + \frac{1}{2} \langle [u + (1 - \epsilon)v]^n \rangle$, giving

$$M_n = \frac{\sum_{k=1}^{n-1} \binom{n}{k} (1 - \epsilon)^k M_{n-k} M_k}{1 - \epsilon^n - (1 - \epsilon)^n}. \quad (23)$$

Since the total field is conserved, the value of M_1 is arbitrary, and we may take $M_1 = 1$, as enforced in the numerical simulations. This yields $\langle u^2 \rangle = 1/\epsilon$, so that the mean width defined according to (17) is $W^2 = M_2 - M_1^2 = \frac{1-\epsilon}{\epsilon}$. Figure 8 proves that this result is correct in the large- ϵL regime.

To test more thoroughly the accuracy of the approximations, in Fig. 9 we compare the mean-field values of the first three nontrivial moments with their numerical values. While the comparison seems to support the main assumption that the neighboring sites are statistically independent, an additional check for this dependence gives a different picture. For a quantitative characterization of the independence of two distributions $w(u_n)$ and $w(u_{n+d})$ at sites separated by a distance d , we use the mutual information

$$I(d) = \sum_{i,j} W_{ij} \log \frac{W_{ij}}{p_i q_j},$$

where p_i and q_j are binned probabilities, and W_{ij} is the joint binned probability. For independent random variables, mutual information vanishes, but in real calculations it is always positive. The values of $I(d)$ for large distances d serve as ‘‘surrogates,’’ giving the numerical level of mutual information for practically independent distributions. The results (Fig. 10)

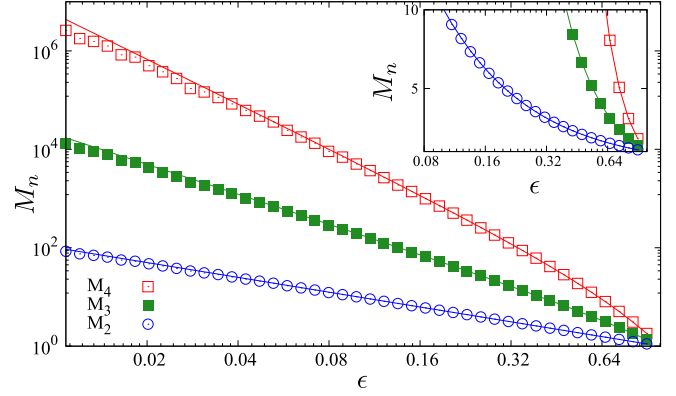


FIG. 9. Comparing numerically found moments 2–4 (markers, in a lattice of $L = 1024$) with theoretical formulas (lines). The inset shows a region of large ϵ with a linear scale of the M_n -axis.

suggest that the independence of neighbors might be *exact* for $\epsilon \geq 0.5$. But, instead, mutual dependence appears for $\epsilon < 0.5$. On the other hand, even for $\epsilon = 0.01$, only some five neighboring sites are interdependent according to the mutual information criterion.

B. Limit of strong microdiffusion $\epsilon \rightarrow 1$

Let us rewrite the local TT model as an application of a matrix,

$$A(\mu, \pm) = \begin{cases} \begin{pmatrix} 1 - \mu & 0 \\ \mu & 1 \end{pmatrix} & \text{prob } 1/2, \\ \begin{pmatrix} 1 & \mu \\ 0 & 1 - \mu \end{pmatrix} & \text{prob } 1/2, \end{cases}$$

where a portion $\mu = 1 - \epsilon$ is moved to the right (to the left). To have a symmetric situation, suppose that this matrix is applied twice (thus, one has four combinations). Furthermore, we assume $\mu \ll 1$, in this case $A(\mu, +)A(\mu, -) \approx$

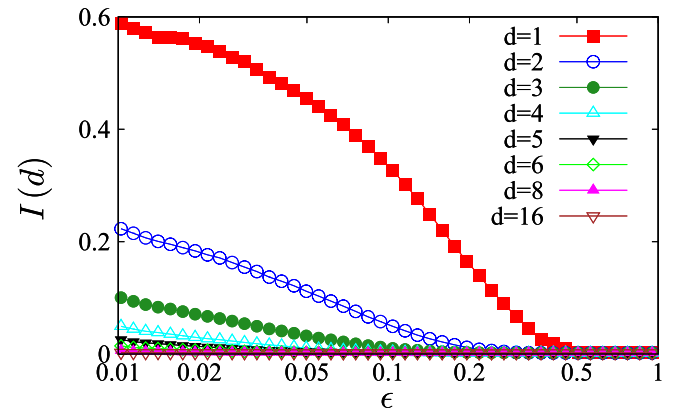


FIG. 10. Mutual information for different distances d between the sites. Details of calculations: $L = 1024$, number of patterns in statistical averaging 1024, number of bins 64 (bins are spaced so that all bins have the same probability $1/64$).

$A(\mu, -)A(\mu, +)$. Then in the first order in μ ,

$$A^2 = \begin{cases} \begin{pmatrix} 1-\mu & \mu \\ \mu & 1-\mu \end{pmatrix} = I + \mu \begin{pmatrix} -1 & 1 \\ 1 & -1 \end{pmatrix} & \text{prob } 1/2, \\ \begin{pmatrix} 1-2\mu & 0 \\ 2\mu & 1 \end{pmatrix} = I + 2\mu \begin{pmatrix} -1 & 0 \\ 1 & 0 \end{pmatrix} & \text{prob } 1/4, \\ \begin{pmatrix} 1 & 2\mu \\ 0 & 1-2\mu \end{pmatrix} = I + 2\mu \begin{pmatrix} 0 & 1 \\ 0 & -1 \end{pmatrix} & \text{prob } 1/4 \end{cases}$$

(here, I is the unit matrix). To obtain a continuous-in-space formulation, we attribute operator ∂_{xx} to the first matrix, and operators $\pm\partial_x$ to the second and third matrices. In this way, we approximate the evolution with

$$\partial_t u(x, t) = \mu \partial_x (Vu) + \mu \partial_{xx} u, \quad V = \pm \frac{\Delta x}{\Delta t}.$$

Because V has independent values at different sites and different time steps, we can model the velocity with a δ -correlated noise field,

$$\begin{aligned} \partial_t u(x, t) &= \mu \partial_x (\xi(x, t)u) + \mu \partial_{xx} u, \\ \langle \xi(x, t) \xi(x', t') \rangle &= \delta(x - x') \delta(t - t'). \end{aligned}$$

Rescaling time $\mu t = \tau$, we obtain

$$\begin{aligned} \partial_\tau u(x, \tau) &= \mu^{1/2} \partial_x (\eta(x, \tau)u) + \partial_{xx} u, \\ \langle \eta(x, \tau) \eta(x', \tau') \rangle &= \delta(x - x') \delta(\tau - \tau'). \end{aligned}$$

Let us suppose that $u = u_0 + \mu^{1/2}u_1 + \mu u_2 \dots$. Substituting this, we get in the leading order

$$\partial_\tau u_0 = \partial_{xx} u_0,$$

which yields a uniform asymptotic state $u_0 = \text{const}$. We suppose $u_0 = 1$, like in the lattice model above.

In the next order, we get

$$\partial_\tau u_1 = \partial_x (\xi(x, \tau)) + \partial_{xx} u_1,$$

which is the conserved version of the Edwards-Wilkinson (EW) equation [21].

Smith *et al.* [51] considered this EW equation and, in particular, demonstrated that the variance diverges (UV catastrophe). They did not perform a cutoff at the lattice size, but from their Eq. (8) it follows that $\text{var}(u_1) \approx \ell^{-1}$, where ℓ is the lattice spacing. The total variance is $\text{var}(u) \approx \mu \ell^{-1}$, in agreement with the result for the lattice model. Furthermore, from Gaussianity of $\xi(x, t)$ it follows that the distribution of u_1 is Gaussian. We show that the field u in the lattice TT model is indeed Gaussian in the limit $\epsilon \rightarrow 1$ in Appendix B. Thus, we conclude that the limit $\epsilon \rightarrow 1$ corresponds to the conserved version of the Edwards-Wilkinson stochastic differential equation.

C. Field distribution

As mentioned above, we can solve Eq. (22) for the field distribution only in a special case in which $\epsilon = 1/2$. Numerical simulations have shown that for $\epsilon < 1/2$, the distribution has a power-law singularity at $u \rightarrow 0$, and cumulative distribution can be well approximated by a stretched exponential with a Gaussian cutoff:

$$P(>u) = \exp[-A(uL)^\alpha - B(uL)^2]. \quad (24)$$

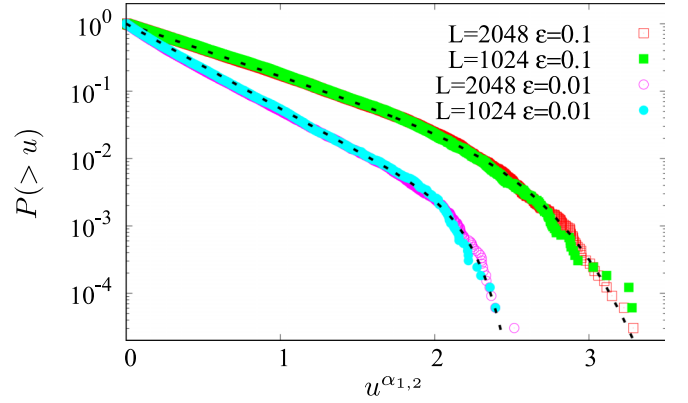


FIG. 11. Cumulative field distributions for $\epsilon = 0.1$ and 0.01 , and different L . Markers are the simulation data, dotted lines are fits with expression (24). For the exponents $\alpha_{1,2}$, the theoretical expression (25) is used.

We illustrate this in Fig. 11, where we show in rescaled coordinates the distributions for $\epsilon = 0.1$ and 0.01 .

Although we cannot derive expression (24), we can estimate the exponent α assuming the validity of (24). Let us suppose that the cumulative distribution $P(>u) = \int_u^\infty w(y) dy$ has the form of a stretched exponential $P(>u) = \exp[-au^\alpha]$ for small u and $\alpha < 1$. Then, the density has a power-law singularity at small u of the form

$$w(u) = a\alpha u^{\alpha-1} \exp[-au^\alpha] \approx Au^{\alpha-1}.$$

Let us look at which value of α is consistent with the Perron-Frobenius equation (22). Substituting, we get

$$\begin{aligned} Au^{\alpha-1} &\approx \frac{1}{2} \frac{A}{\epsilon} \frac{u^{\alpha-1}}{\epsilon^{\alpha-1}} \\ &+ \frac{A}{2\epsilon} \int_0^{u/(1-\epsilon)} A^2 [u - (1-\epsilon)v]^{\alpha-1} v^{\alpha-1} dv \\ &= \frac{Au^{\alpha-1}}{2\epsilon^\alpha} + \frac{A^2}{2(1-\epsilon)^\alpha} u^{2\alpha-1} \int_0^1 (1-z)^{\alpha-1} z^{\alpha-1} dz. \end{aligned}$$

Neglecting the last term, we obtain the consistency condition $2\epsilon^\alpha = 1$ which means

$$\alpha = -\frac{\log 2}{\log \epsilon}. \quad (25)$$

This equation is in excellent agreement with the numerics as shown in Fig. 12.

D. Time correlations

In this section, we discuss the one-site temporal correlation function of the field (remember that we set $\langle u \rangle = 1$),

$$C(\Delta t) = \langle [u_n(t) - 1][u_n(t + \Delta t) - 1] \rangle.$$

The calculated time-correlation function is shown in panel (a) of Fig. 13. It appears that the correlations decay as a power law $(\Delta t)^{-1/2}$. In contrast, for $L = 2$ the decay is exponential [see Appendix A and the panel (b) of Fig. 13]. Thus, one can expect a crossover at small L . We show in Fig. 13(b) how correlations for a fixed $\epsilon = 0.6$ depend on L . Here scaled coordinates are used; one can see that starting from $L =$

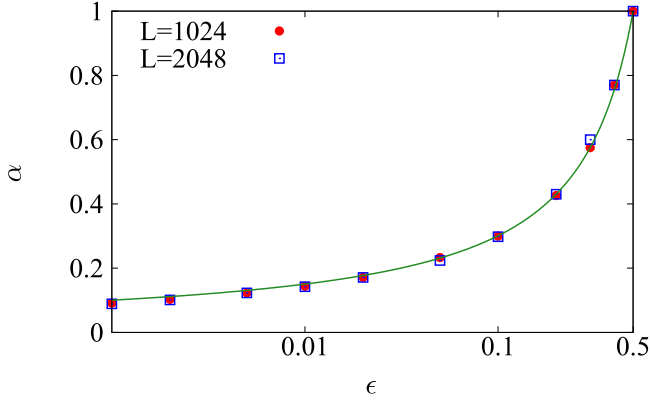


FIG. 12. Numerical values of the exponent α of the stretched-exponential part of the cumulative distribution (24) as a function of ϵ (markers) together with the analytic estimate, Eq. (25).

4, the scaling law $C(\Delta t) \approx L^{-1} b(\Delta t L^2)^{-1/2} \exp[-a\Delta t L^2]$ works well (fitted values for a , b are in the caption).

VII. WEAK MICRODIFFUSION $\epsilon < L^{-1}$

A. Hierarchical structure of peaks

We start our treatment of the case of very small microdiffusion with a visualization in Fig. 14(a) of a snapshot of a field $\{u_k\}$ in a statistically stationary regime (i.e., at times larger than characteristic transient time L^2), at small values of microdiffusion parameter ϵ . At $\epsilon = 0$, the field is just one peak (the maximal cluster) at which the whole initial “mass” is concentrated, at a random spatial position. For better compar-

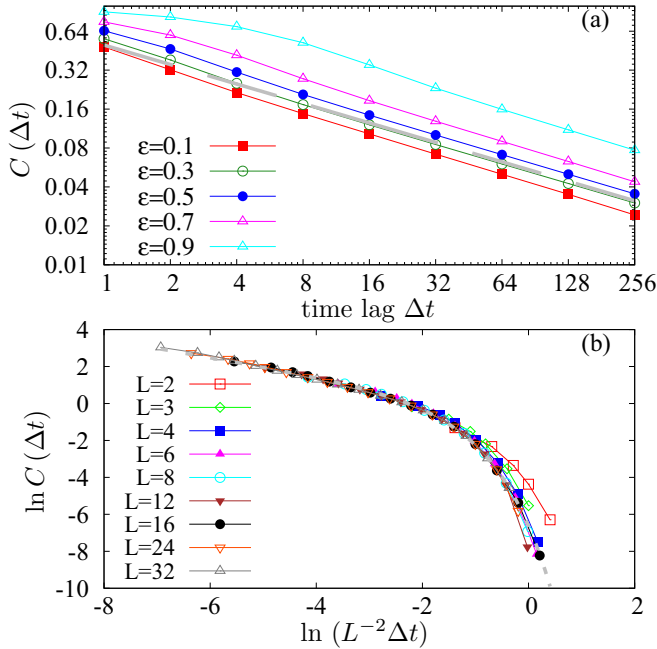


FIG. 13. (a) Time-correlation functions for a lattice of length $L = 1024$ and different ϵ . The dashed gray line on this panel has a slope of $-1/2$. (b) Time-correlations in scaling coordinates for different L and $\epsilon = 0.6$. The dashed gray line is a fit $\log y = -0.511 - 0.5 \log x - 6.122 \exp(x)$.

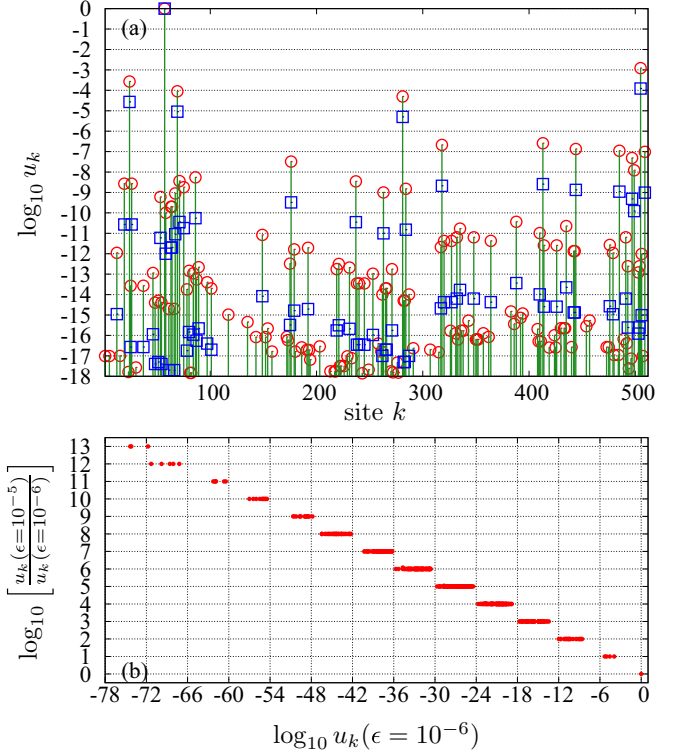


FIG. 14. (a) Snapshots of the fields with $\epsilon = 10^{-5}$ (red circles) and $\epsilon = 10^{-6}$ (blue squares) for $L = 512$. Green vertical lines show the positions of the main peaks (i.e., those with markers; there are many other peaks with masses smaller than 10^{-18} ; cf. the bottom panel). (b) The logarithmic difference in the levels of the peaks [i.e., the distance between red circles and blue squares of panel (a) at each peak] vs the level of the blue squares.

ison of fields for different sizes of the lattice L , we use below the normalization $\sum_k u_k = 1$; thus, the single peak for $\epsilon = 0$ has mass 1. Together with this maximal cluster, one observes in Fig. 14(a) peaks at different levels with a strong separation (several orders) between them.

To qualitatively understand this hierarchical structure of the field (which we will quantitatively characterize below), let us start with a single peak at $\epsilon = 0$ and switch to a finite but small value of ϵ . Then, the randomly moving main peak will leave behind secondary peaks of mass $\approx \epsilon$. These peaks will also move, leaving the next generation of peaks of mass $\approx \epsilon^2$; they can also merge and be absorbed by the main peak (the size of which remains close to 1—this is where the condition $\epsilon L < 1$ plays its role). Thus, one can expect peaks at levels $\sim \epsilon$, $\sim \epsilon^2$, $\sim \epsilon^3$, \dots . However, this hierarchy is not very distinct, although recognizable, in the single profile at fixed ϵ ; see the set of red circles or of blue squares in Fig. 14(a). To separate different levels in a more apparent way, we perform a simultaneous run of the TT model at two different values of parameter ϵ : ϵ_1 and ϵ_2 . This means that the same random choices for advection steps (11) are chosen in two runs. As a result, the peaks in the two runs coincide in position but differ in their height by a factor $(\epsilon_1/\epsilon_2)^m$ with integer m . For an illustration in Fig. 14(a) we have chosen $L = 512$, $\epsilon_1 = 10^{-5}$ (red circles), and $\epsilon_2 = 10^{-6}$ (blue squares). The grid in the y -axis corresponds to the ratio $\epsilon_1/\epsilon_2 = 10$. One

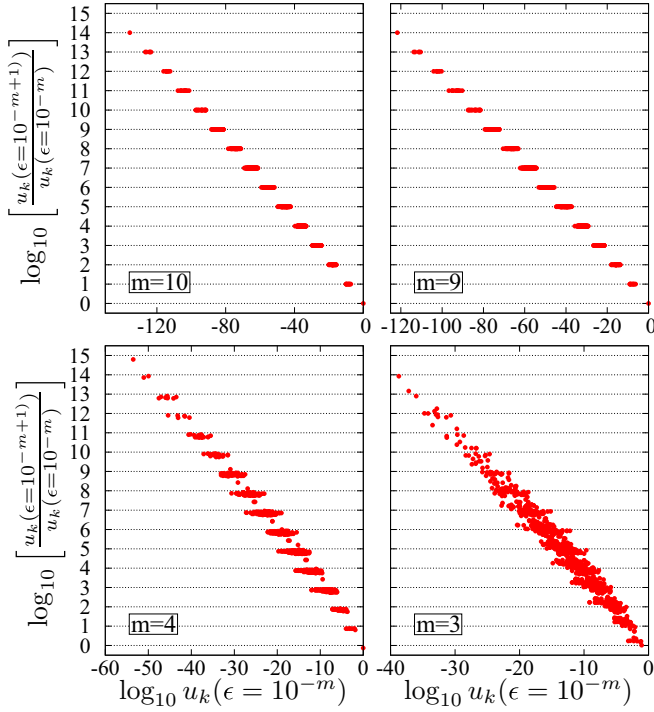


FIG. 15. The same plots as in Fig. 14(b), but for different values of $\epsilon = 10^{-m}$. One can see that for large ϵ the order structure becomes blurry, and eventually no clear separation is seen for large ϵ .

can see that the main peaks in the two runs coincide. There are four peaks at the next level, with a separation between them by a factor $\epsilon_1/\epsilon_2 = 10$. The number of peaks at the next level is larger; there, the separation is $(\epsilon_1/\epsilon_2)^2 = 100$, etc. To make the correspondence of the separation and the level apparent, we plot in Fig. 14(b) all the $L = 512$ values of $\{u_k\}$ from the snapshot Fig. 14(a) in the coordinates “mass versus separation” (both axes are logarithmic). One can see that the separations are very well “discretized” at integers of $\log_{10}(\epsilon_1/\epsilon_2)$ (y-axis), while the levels in the field values are spread much wider (x-axis), and these widths for deep levels are of the same order as $-\log_{10} \epsilon_2 = 6$.

To illustrate that this hierarchical structure appears for small enough ϵ only, we show in Fig. 15 the same plots as Fig. 14(b) for $L = 1024$ and different values of $\epsilon_1 = 10^{-m}$ and $\epsilon_2 = 10\epsilon_1$. One can see that the separation is apparent for $m = 10, 9$ but becomes less distinct for $m = 4$ and is practically not seen for large ϵ ($m = 3$).

B. Order kinetic model

In this section, we present an effective model [termed the order kinetic model (OKM)] to describe the structure observed in the simulation for small ϵ ; see Figs. 14 and 15. Motivated by the observed hierarchical structure, we attribute to each site k an integer-valued order μ_k , and we assume that the field u_k is represented as

$$u_k \approx \rho \epsilon^{\mu_k}. \quad (26)$$

Here $\mu_k \geq 0$ is an integer called the “order” of the field at site k . Parameter $\rho \approx 1$ is a normalization factor [it corresponds roughly to the mass of the (unique) site having zero order

in the asymptotic steady state]. In the following, we will refer to the sites having the same value of μ as the peaks of order μ , and we denote by $n(\mu)$ their number and by $p(\mu) = n(\mu)/L$ their fraction (i.e., the probability to observe specific order). The expression (26) corresponds to an approximation in which the horizontal steps in Fig. 14(b) have zero width and zero height.

Let us now rewrite the update rule (11) in terms of the orders μ_k by considering two neighboring sites (i, j) corresponding, respectively, to orders (μ_i, μ_j) , with the direction of advection $i \rightarrow j$. Since the mass $(1 - \epsilon)u_i$ is transferred to site j and the mass ϵu_i is left to site i , we write the following update rule for the orders:

$$\begin{aligned} \mu_i &\rightarrow \mu_i + 1, \\ \mu_j &\rightarrow \text{MIN}\{\mu_i, \mu_j\}. \end{aligned} \quad (27)$$

The approximation here follows from our perfect discretization of the levels: we neglect changes in the field if the addition is smaller than the existing field by a factor ϵ^m , $m \geq 0$.

Special care should be taken about the sites with minimal possible order, $\mu_{\min} = 0$. As it follows from (27), the number of such sites can only decrease, and eventually there is only one such site in the lattice. With one site having zero order, this situation is an absorbing state in model (27).

Before proceeding, we notice that the OKM (27) is, in fact, a skew (unidirectionally coupled) system: Higher-order peaks do not influence the zero-order peak; the first-order peaks interact only with each other (can coalesce) and with the zero-order peak (they can be “emitted” or “absorbed” by it), etc. We will use this property in Sec. VIII D below.

C. Mean-field approach

In the framework of the OKM, one can apply the same mean-field approach as in Sec. VI A to write an equation for the evolution of the probabilities $p(\mu)$. The basic assumption is the independence of neighboring values of $\mu_{i,j}$ in (27). Thus, the minimum (MIN) in (27) should be calculated as a minimum value of two independent random variables having the same distribution $p(\mu)$:

$$\begin{aligned} \text{prob}(\text{MIN}(\mu_i, \mu_j) > \mu) &= \text{prob}(\mu_i > \mu) \text{prob}(\mu_j > \mu) \\ &= (1 - \text{prob}(\mu_i \leq \mu)) (1 - \text{prob}(\mu_j \leq \mu)). \end{aligned}$$

This leads to the following expression for this distribution, valid for $\mu \geq 1$ [this expression is analogous to (22)]:

$$\begin{aligned} p(\mu) &= \frac{1}{2} p(\mu - 1) \\ &+ \frac{1}{2} \left[\left(1 - \sum_{v=0}^{\mu-1} p(v) \right)^2 - \left(1 - \sum_{v=0}^{\mu} p(v) \right)^2 \right]. \end{aligned} \quad (28)$$

The first term corresponds to the case in which the site is a “source” (this happens with probability 1/2); the second term corresponds to the case (also with probability 1/2) when the site is a “destination.” One can see from (28) that $p(\mu)$ depends only on values $p(v)$ with $v < \mu$. In terms of $p(\mu)$, expression (28) is a quadratic equation. Its solution begets a

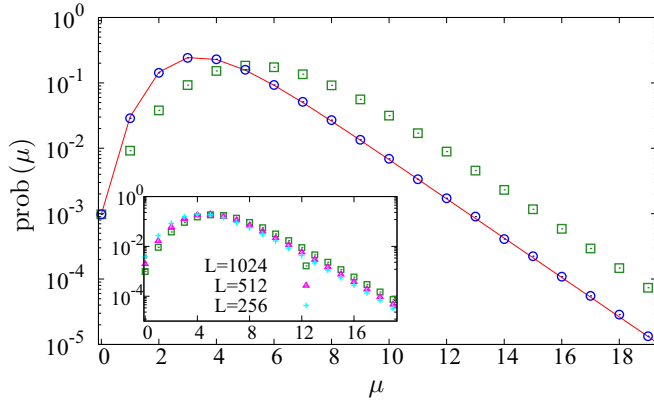


FIG. 16. Comparison of a theoretically obtained distribution of peaks $p(\mu)$ [Eq. (29), red curve] with numerics for the TT model (green squares) and for the global coupled TT model (12), blue circles. All these data are for $L = 1024$. In the inset, we also show data for the TT model with $L = 512$ and 256 .

recursion relation

$$p(\mu) = \sqrt{s^2(\mu - 1) + p(\mu - 1)} - s(\mu - 1),$$

$$s(\mu) = \sum_{\nu=0}^{\mu} p(\nu), \tag{29}$$

which has to be iterated starting from $p(0) = 1/L$. We compare this solution with a numerically obtained distribution in Fig. 16. One can see that the correspondence is not good, which indicates that in the TT model (11) the correlations between the neighboring sites are large and cannot be neglected. On the other hand, for the global coupled version of the TT model (12), where correlations are expected to be very small in the thermodynamic limit, the correspondence is very good.

D. Dynamics of lowest-order peaks

As demonstrated above, for the OKM the mean-field approximation is not very successful because of correlations in the peak positions. Such a correlation is not very surprising because the first-order peaks are “daughters” of the zero-order peak and thus are located close to it; the same holds for other orders (“The apple never falls far from the tree”). To get insight, we visualize the dynamics of the peaks of orders $\mu = 0, 1, 2$. In Fig. 17, we compare the trajectories of the main (zeroth-order) peak (blue) with those of the peaks of order 1 (red) and 2 (green). One can clearly see that the first-order peaks are mainly in the vicinity of the zero-order peak (from which they are created), but some leave this vicinity, diffuse, and merge. A similar creation-merging is observed at the bottom panel, where peaks of order 1 and 2 are depicted.

Let us now describe the relative motion of the main peak and the first-order peaks. To this aim, let us focus on Fig. 17 (middle panel), which shows the main peak (order 0) and the peaks of order 1. Let us redraw this figure by plotting the differences in the positions of the peaks of order 1 and the position of order 0; see Fig. 18 (in fact, here, another random realization is taken).

To describe Fig. 18, we can formulate a reduced version of the OKM (27), which takes into account only peaks of the

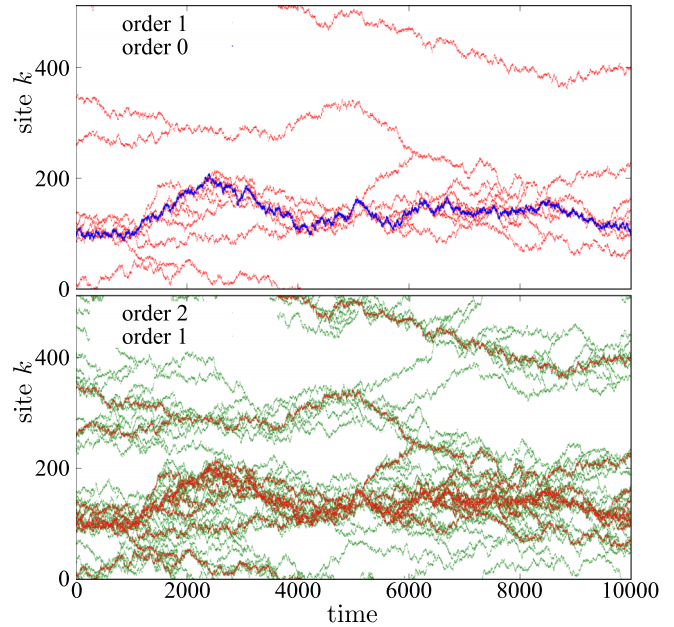


FIG. 17. Trajectories of peaks of orders 0 (blue, dark) and 1 (red, middle dark) (top panel), and of orders 1 (red, middle dark) and 2 (green, light gray) (bottom panel) [simulations of the TT model (11) for $L = 512$, $\epsilon = 10^{-6}$]. Simulations were started from random initial conditions, but an initial transient of duration L^2 was dismissed.

first order (we denote their masses as w_k) and the main one (zero-order peak). Moreover, it is instructive to go beyond the OKF and distinguish masses of the first-order peaks (although later, we will ignore them). Because the motions of the main peak and of other sites are independent, we place the main peak at zero and fix it. The dynamics of all other sites follows the KR model (TT model with $\epsilon = 0$). Namely, at time t , a pair of points k, l is chosen randomly, with $l = k \pm 1$. If $k = 0$, then we set $w_l(t + 1) = w_l(t) + 1$. If $k \neq 0$ and $l \neq 0$, then the dynamics is as follows:

$$w_k(t + 1) = 0, \quad w_l(t + 1) = w_l(t) + w_k(t).$$

If $k \neq 0$ and $l = 0$, then $w_k(t + 1) = 0$. This dynamics can be described as follows: The mass of the main peak (located

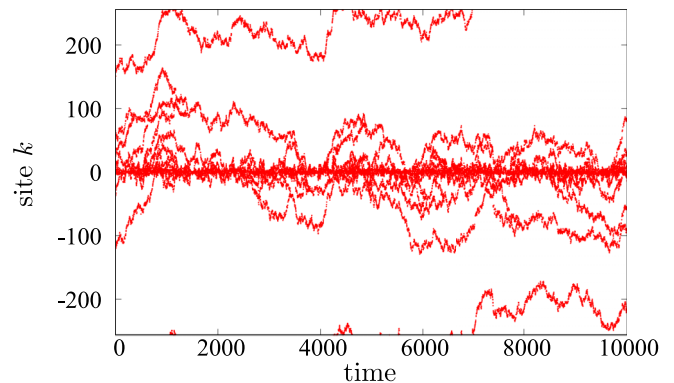


FIG. 18. Trajectories of the distances of the peaks of level one from the main peak for $L = 512$ (thus, the position of the main peak is at zero) in the TT model (11).

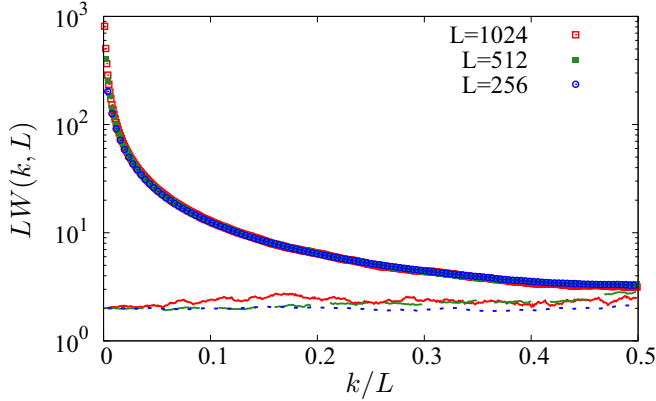


FIG. 19. Occupation densities $W(k, L)$ (markers) of the first-order peaks along the lattice for different L , in the scaled coordinates LW vs k/L . In this panel, the curves (red solid, $L = 1024$; green dashed, $L = 512$; blue dotted, $L = 256$) are non-normalized mass densities ρ vs k/L .

at the origin) is not varied. Instead, this peak randomly emits “daughters” of mass 1. These first-order particles diffuse and coalesce. They disappear when the main peak absorbs them.

This model yields positions of the first-order peaks that crowd around the main peak but can also leave its vicinity, making excursions to the “bulk” of the lattice. Note also that the model is not space-shift invariant because we fix the main peak at the origin.

To characterize the crowding, it is important to distinguish two types of densities. One is $\rho(k) = \langle w(\pm k, t) \rangle$ (here because of symmetry around zero, sites $\pm k$ are considered equivalent). This is an average mass; peaks with higher mass (after one or several coalescence events) contribute more to this density.

Another density is $W(k, t) = \langle 1 - \delta(w(\pm k, t)) \rangle$, where $\delta(w) = 1$ if $w > 0$ and $\delta(w) = 0$ if $w = 0$. This density counts occupied sites, irrespective of the value of the mass w at these sites.

Because the motion of the peaks between interactions with the main peak at the origin is a pure diffusion, one expects that the stationary mass density $\rho(k)$ is uniform. On the other hand, the occupation density $W(k)$ decays due to collisions with other first-order peaks, thus one expects that in the stationary state, it is maximal close to the origin and decays toward the bulk of the lattice.

We elaborate on statistical theory for the occupation density $W(k, t)$ in Appendix C. This theory predicts that the stationary density scales with the lattice size L as $W(k) = L^{-1} \hat{W}(k/L)$. This relation is tested in Fig. 19. We also confirm that $\rho(k)$ is uniform in this figure.

Another prediction is that the average number of the first-order peaks grows with the lattice size as $\sim \log L$; this relation is checked in Fig. 20. For higher-order peaks, the dependence on $\log L$ is nonlinear (not shown).

VIII. DISCUSSION AND CONCLUSIONS

We start by summarizing our main findings. We have studied the statistical properties of KR and TT lattice models. The

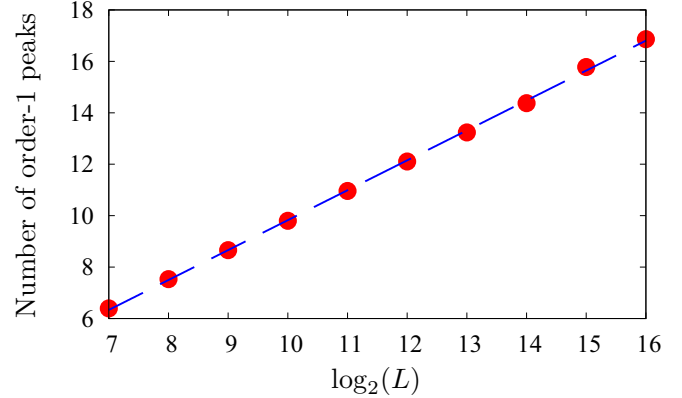


FIG. 20. Mean number of order-1 peaks as a function of lattice size L (markers). The dashed line is a linear fit.

only two parameters are the redistribution constant ϵ and the lattice size L . There are two main regimes: $\epsilon \lesssim L^{-1}$, where microdiffusion is small, and $\epsilon \gtrsim L^{-1}$, where microdiffusion is large. For small microdiffusion, one observes a concentration of almost all mass on a single randomly moving site (this concentration is perfect in the KR case, $\epsilon = 0$). The masses on other sites are small, and for very small ϵ , the dynamics build a hierarchical structure, described in detail in Sec. VII. For large microdiffusion, a random regime that is statistically uniform in space is established, as described in Sec. VI. In the limit $\epsilon \rightarrow 1$, this regime corresponds to the Edward-Wilkinson equation with conserved noise.

It is instructive to compare the properties of the KR and TT models to other cases from the literature where mass-conserved models, which can be interpreted as advection/transport on a one-dimensional lattice (some with condensation/coagulation), have been studied.

The foremost feature of all models studied in this paper and summarized in Fig. 2 is that the average density ρ is a scalable parameter; therefore, it cannot act like a control parameter, and no (equilibrium or out-of-equilibrium) phase transition can appear when tuning ρ , not even at $\rho = 0$, because the model is not defined in the absence of mass. This property is, of course, shared with the random advection-diffusion equation (6).

Nonetheless, it is interesting to analyze our models in terms of *condensation*, a process occurring when a finite fraction of the total mass/energy is localized on a finite number of sites; in our language, this corresponds to the formation of a maximal cluster.

Adopting a strict point of view according to which a phase transition only occurs in the thermodynamic limit, the only model displaying condensation is KR, whose steady state corresponds to a single site hosting the whole mass. However, considering the mass distribution at finite size L , the TT model has remarkable features because the degree of condensation depends on the product of the intensive parameter ϵ and the extensive parameter L : we have a sort of finite-size condensation for lattices with $L \lesssim 1/\epsilon$. On this scale (which diverges for $\epsilon \rightarrow 0$), almost all mass is concentrated on a single site (a zero-order peak), as described in Sec. VII.

We add that such finite-size condensation is attained via a dynamic coarsening, in which the condensed fraction increases with time. This phenomenon is visible as the increase of roughness over time, as described in Sec. V.

When comparing different models, the deterministic versus random rule to redistribute the mass is an important feature. In the TT model, the parameter ϵ is fixed, but it could be chosen randomly in the unitary interval, obtaining effectively the “random TT model,” which has been studied (although not with this name) by Rajesh and Majumdar in Ref. [35] (it corresponds to their symmetric model in the limit of continuous-time dynamics). Thus we denoted it as RM in Sec. III A. The phenomenology of such a model is fairly different from ours, which is strongly dependent on ϵL , a parameter that is meaningless if ϵ is random.

It is also instructive to compare with the Kipnis-Marchioro-Presutti (KMP) model [34], where a pair of sites $(k, k \pm 1)$ is chosen randomly, and the masses are redistributed according to

$$u'_k = \xi(u_k + u_{k\pm 1}), \quad u'_{k\pm 1} = (1 - \xi)(u_k + u_{k\pm 1}), \quad (30)$$

ξ being a random number uniformly distributed in $(0, 1]$. In Ref. [34], it has been proven that a stationary distribution in the KMP model is an equilibrium Gibbs distribution. This is not surprising because the update rule (30) satisfies the detailed balance condition. This is in contradistinction to the TT model (even in its random version), where the detailed balance is not valid. KMP is the prototypical example of diffusion, and therefore of a smoothing process. It is interesting, therefore, to consider its deterministic counterpart (det-KMP in Sec. III A), where ξ is fixed, and we denote $\xi = \epsilon$. In the limit $\epsilon = 0$, it is the same as the KR model; we might therefore think that for small ϵ it is similar to the TT model. Before considering this possibility, we should note that the det-KMP model is invariant under the transformation $\epsilon \rightarrow 1 - \epsilon$, which sets $1/2$ as the maximal value of ϵ . For this reason, when reproducing Fig. 8 for the det-KMP model, we have replaced $\epsilon/(1 - \epsilon)$ (see the label of the horizontal axis) with $\epsilon/(0.5 - \epsilon)$. The result is plotted in Fig. 21, showing a strong resemblance between the two *deterministic* models. We emphasize “deterministic” to stress that the TT model is far more similar to det-KMP than to the random version of itself (RM).

It is worth stressing a further difference between the finite-size localization found in TT and det-KMP and the standard condensation process found in models where the density ρ (density of mass or other conserved quantity) plays the role of the control parameter. There are many such models, but we will not review them here. We will simply say that condensation exists if ρ is larger than some critical value ρ_c (we will give a specific example later). Let us now try to make a connection between the standard condensed phase appearing for $\rho > \rho_c$ and the finite-size localized phase found in TT and det-KMP models when $\epsilon < \epsilon_c = 1/L$. In both cases, we have a condensate in equilibrium with a background, and, for large L , the condensate is composed of a single site hosting a macroscopically large peak. Let us now imagine removing the condensate: in the TT model the density is scalable, and a new condensate will spontaneously appear. Instead, in the standard condensation models, this will not occur because removing the condensate will also reduce the density to its

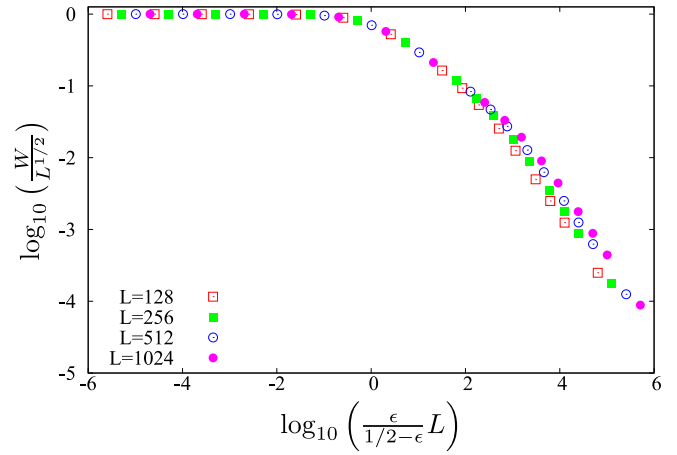


FIG. 21. Saturated width of the interface in the det-KMP model in scaled coordinates, for different ϵ and different lattice sizes. This plot is very similar to Fig. 8, suggesting that the det-KMP model probably has the same statistical properties as the TT model.

critical value, $\rho \rightarrow \rho_c$. We stress that this is not just a trivial reformulation due to the different physical nature of the two control parameters ρ and ϵ (a “density” versus “not a density”), rather it is a consequence of a different dynamical behavior in the condensed phase. In standard condensation models, the condensate and the background belong to two different equilibrium phases, and the removal of the condensate does not affect the background. In the TT model, there is really no such distinction, as clarified by the order kinetic model discussed above.

To obtain a standard condensation transition where the density plays the role of a control parameter, it is necessary to introduce a physical scale of the mass. For this reason, we conclude this discussion by mentioning a chipping model (CM) [52,53] where the mass u_i is a non-negative integer and which seems to have some features similar to the TT model. Here mass is transported (advected) symmetrically to one of the neighboring sites with two distinct and parallel processes: (i) The whole mass (i.e., all particles) is transported from site i to site $i \pm 1$ (this corresponds to advection, or macrodiffusion). This occurs with rate 1. (ii) One single particle (if it exists) is transported from site i to site $i \pm 1$ (this corresponds to microdiffusion). This occurs with rate w . This model displays condensation for $\rho > \rho_c = \sqrt{1 + w} - 1$.

If $w = 0$, then $\rho_c = 0$, and this model is equivalent to the KR model, displaying the formation of a single cluster containing all the mass. If $\rho \gg 1$, the discrete nature of the mass is not relevant, and for diverging w CM is similar to the TT model for $(1 - \epsilon) \ll 1$, which explains why it does not display condensation. The CM model is another simple example of a lattice with a clear separation of micro- and macrodiffusion: for $w = 0$ there is only macrodiffusion, while for $w = \infty$ there is only microdiffusion. For finite values of w , their relative importance depends on the mass density.

In this manuscript, we have proposed a unifying picture to gather several models of local mass transport under the same umbrella; see Fig. 2. It seems to us that different models, including models not covered by such an umbrella, e.g., the just-mentioned CM model, might be discussed in terms of

micro/macrodifusion, macrodifusion being a key element in obtaining a condensation-like phenomenon, and microdifusion being the obstacle to it. In particular, we have discussed in detail a deterministic process in which a single parameter ϵ allows us to switch between the two cases.

Since we have shown that the deterministic or random nature of the parameters a, b entering in the definition of the generic two-site model, see Sec. III A, is of crucial importance, it might be of interest to distinguish between these two classes and determine the ensemble of models of each class displaying condensation.

Another challenging problem for future studies is an extension of the above-mentioned models to two- and three-dimensional lattices (cf. [27] for studies of particles sliding along two-dimensional surfaces). Here already the phenomenology of pure random advection is nontrivial, as depending on the sign of the maximal Lyapunov exponent, one can observe in the absence of microdifusion either a single cluster (a δ -distribution of density as in one-dimensional case) or a random fractal. It is not clear how the latter case can be modeled on a lattice.

Finally, we mention that a possible experimental setup where the statistics of one-dimensional random advection can be studied is that of particles floating on the surface of fluid where one-dimensional wave turbulence is realized [8,54]. While natural turbulence has quite specific statistical properties (that of the Kolmogorov-Zakharov spectrum [29]), a more random field could potentially be created via external random driving. It might, however, happen that in such an experiment the cluster size will be affected not by microdifusion, but by the finite sizes of the particles.

ACKNOWLEDGMENTS

We thank P. Grassberger for valuable discussions. A.P. acknowledges the hospitality of ISC-CNR in Florence. P.P. and S.L. acknowledge support from the MIUR PRIN 2017 project 201798CZLJ.

APPENDIX A: THE TT MODEL AS AN IFS

In this Appendix, we demonstrate the fractal properties of the invariant distribution in the TT (11) model for small lattice lengths, adopting the iterated function systems (IFSs) concept.

1. Case $L = 2$: Bernoulli convolution

Let us consider the minimal case $L = 2$ and $u_1 + u_2 = 2$. Because of the conservation law, we have just one nontrivial variable u , since another variable is expressed as $2 - u$. In this case, the transformation (21) reads

$$u(t+1) = \begin{cases} \epsilon u(t) & \text{Prob } 1/2, \\ \epsilon u(t) + 2(1-\epsilon) & \text{Prob } 1/2. \end{cases} \quad (\text{A1})$$

This one-dimensional IFS is the so-called Bernoulli convolution [55–57]. Bernoulli convolution generates a classical fractal if $\epsilon < 1/2$, and a relatively smooth distribution without voids for $\epsilon > 1/2$; see [58,59]. [For $\epsilon = 1/2$, the invariant distribution is uniform.] The expression for the dimension (there is only one dimension for $\epsilon < 1/2$; the set is a mono-fractal)

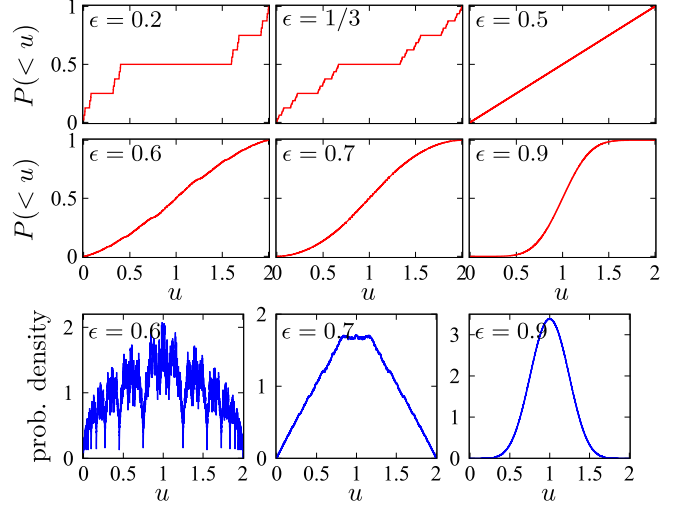


FIG. 22. The cumulative distribution $P(<u)$ in the IFS system (A1) for different ϵ (upper two panels). This distribution is a classical fractal for $\epsilon < 1/2$. The distribution is continuous for $\epsilon > 1/2$ but becomes smooth only for large ϵ . Bottom panel: densities for cases $\epsilon > 1/2$.

is a trivial application of the scaling relation: $d = -\frac{\log 2}{\log \epsilon}$, and it is smaller than 1 for $\epsilon < 1/2$. In Fig. 22, fractal and smooth examples are presented [58,59].

It is straightforward, using linearity of (A1), to calculate the statistical properties of $u(t)$ (cf. [60]). The average is $\langle u \rangle = 1$. For the autocorrelation function $C(t) = \langle [u(t) - 1][u(0) - 1] \rangle$ one easily obtains a recursion $C(t+1) = \epsilon C(t)$, from which the exponential decay of correlations follows, $C(t) = C(0)\epsilon^t$.

2. Case $L = 3$

In this case, because of the conservation law $u_1 + u_2 + u_3 = 3$, the dynamics lies on a two-dimensional simplex. Several images of the distribution (10^4 points are drawn) are shown in Fig. 23. As in the $L = 2$ case, the distribution is without voids for $\epsilon \geq 0.5$ and a fractal measure with a hierarchy of voids for $\epsilon < 0.5$.

APPENDIX B: GAUSSIANITY OF THE FIELD DISTRIBUTION IN THE LIMIT $\epsilon \rightarrow 1$

Here we rewrite the TT model using $\mu = 1 - \epsilon \ll 1$:

$$\bar{u} = \begin{cases} (1-\mu)u & \text{prob } 1/2, \\ u + \mu u_{\pm} & \text{prob } 1/2. \end{cases}$$

Let us introduce the characteristic function $C(k) = \langle e^{iku} \rangle$ and assume that u and u_{\pm} are statistically independent. Then the Perron-Frobenius equation for C reads

$$\bar{C}(k) = \frac{1}{2}C[k(1-\mu)] + \frac{1}{2}C(k)C(k\mu).$$

In the stationary situation, $\bar{C} = C$, and we obtain

$$2 = C(\mu k) + \frac{C[(1-\mu)k]}{C(k)}. \quad (\text{B1})$$

Because the mean value of u is arbitrary, we set it to 1. Then the characteristic function can be written in terms of

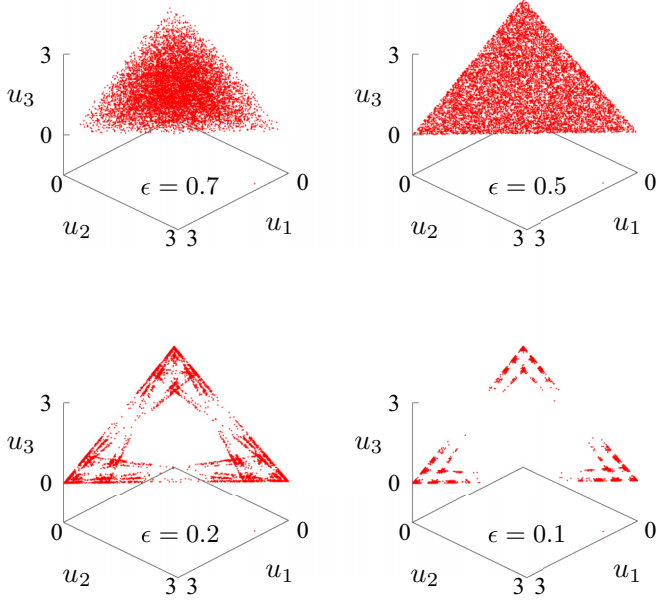


FIG. 23. Distributions of fields (u_1, u_2, u_3) for $L = 3$ and several values of ϵ .

cumulants κ_m , $m \geq 2$:

$$C(k) = \exp \left[ik + \sum_{m=2}^{\infty} \kappa_m \frac{k^m}{m!} \right].$$

For the ratio of characteristic functions, we get

$$\frac{C[(1-\mu)k]}{C(k)} = \exp \left[-ik\mu + \kappa_2 \frac{k^2}{2} (-2\mu + \mu^2) + \kappa_3 \frac{k^3}{6} (-3\mu + 3\mu^2 - \mu^3) + \dots \right].$$

The equation for C (B1) then reads

$$2 = \exp \left[-ik\mu + \kappa_2 \frac{k^2}{2} (-2\mu + \mu^2) + \kappa_3 \frac{k^3}{6} (-3\mu + 3\mu^2 - \mu^3) + \dots \right] + \exp \left[ik\mu + \kappa_2 \mu^2 \frac{k^2}{2} + \kappa_3 \mu^3 \frac{k^3}{6} + \dots \right].$$

We now expand the r.h.s. keeping orders μ^0, μ^1, μ^2 only:

$$2 = 2 + \mu \left[-\kappa_2 k^2 - \kappa_3 \frac{k^3}{2} - \kappa_4 \frac{k^4}{6} - \dots \right] - \mu^2 k^2 + \mu^2 \left[\kappa_2 \frac{k^2}{2} + \kappa_3 \frac{k^3}{2} + \kappa_4 \frac{k^4}{4} + \dots \right].$$

Comparing terms at k^2 , in the leading order in μ we obtain $\kappa_2 = \mu$. Comparing terms at k^3, k^4, \dots we obtain $\kappa_3 = \kappa_4 = \dots = 0$. This proves that for $\mu \rightarrow 0$ the field is Gaussian, with a variance $\kappa_2 = \mu$.

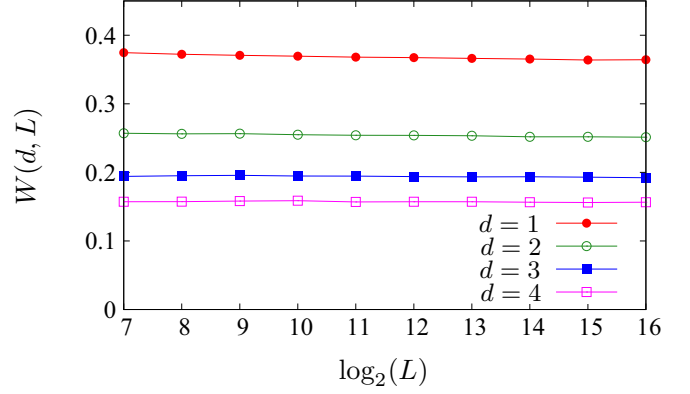


FIG. 24. Mean occupations of the sites $W(k=d)$ close to the main peak (which is at $k=0$) for different sizes of the lattice L . The closest neighbor site has occupation ≈ 0.37 .

APPENDIX C: STATISTICAL THEORY FOR THE OCCUPATION DENSITY OF FIRST-ORDER PEAKS

Here we derive, within the OKM, an equation for the evolution of the occupation density of first-order peaks (treated as particles) $W(k, t)$, in a lattice of length L . First, we replace k with a continuous coordinate $0 \leq x \leq L$. The basic dynamics is a diffusion of particles; thus, we start with the diffusion equation $\partial_t W(x, t) = D \partial_{xx} W(x, t)$.

Due to the coalescence of particles, the number of occupation sites decreases. Therefore, one should add a damping term. To elaborate on this, consider a spatially homogeneous state with constant density W . Then the distance between the particles is $X \approx W^{-1}$. The time for two particles to coalesce is the diffusion time for the distance between the peaks, i.e., $t_c \approx X^2/D$. The rate of coalescence is therefore $t_c^{-1} = DX^{-2} = DW^2$. Thus from the equation $\partial_t (\ln W) = -DW^2$ we get the damping term $\partial_t W = -DW^3$. We notice that the spatially homogeneous solution $W(t) = \frac{W(0)}{\sqrt{1+2DW^2(0)(t-t_0)}}$ yields the asymptotic time dependence $W \sim t^{-1/2}$, which is confirmed by numerics.

However, in our case the occupation density is inhomogeneous because particles are created at $x=0$ (or, equivalently, at $x=L$), where the main peak is placed. The sites near the main peak are predominantly occupied; therefore, we can assume a constant occupation $W=c$ at this boundary. To check that the density at the boundary does not depend on L , we calculated this density numerically at sites adjacent to the main peak in the TT model; see the results in Fig. 24. This figure shows that the occupation of the nearest neighbor to the peak is around 0.37, almost independent of L .

Summarizing, we have the following PDE and boundary conditions for the occupation density $W(x, t)$:

$$\frac{\partial W(x, t)}{\partial t} = D \frac{\partial^2 W}{\partial x^2} - DW^3, \quad W(0, t) = W(L, t) = c$$

for some $c > 0$. The stationary solution $W(x)$ of this equation obeys

$$\frac{d^2 W}{dx^2} - W^3 = 0, \quad W(0) = W(L) = c.$$

We can integrate once and obtain

$$\frac{1}{2} \left(\frac{dW}{dx} \right)^2 - \frac{1}{4} W^4 = -\frac{w^4}{4}, \quad \frac{dW}{dx} = \pm \frac{1}{\sqrt{2}} \sqrt{W^4 - w^4}, \quad (\text{C1})$$

where we took as a constant $w = W_{\min} = W(L/2)$. Integration of this equation on the interval $0 \leq x \leq L/2$ yields

$$\frac{wL}{2\sqrt{2}} = \int_1^{cw^{-1}} \frac{dy}{\sqrt{y^4 - 1}} = \frac{1}{\sqrt{2}} F \left(\arccos \frac{w}{c}, \sqrt{2}/2 \right),$$

where $F(\phi, k)$ is the elliptic integral of the first kind. The constant w should be obtained self-consistently from this relation. If we assume $w \ll 1$, which is to be expected for large lattice sizes L , then $F(0, k) = \pi/2$ and we get a relation

$$wL = \pi.$$

Substituting this in (C1), we can represent the stationary occupation density as $W(x) = \frac{\pi}{L} Q(\frac{x}{L})$, where $Q(z)$ is a solution of ODE $\frac{dQ}{dz} = -\pi 2^{-1/2} \sqrt{Q^4 - 1}$ with initial condition $Q(0) = cL\pi^{-1}$. This relation agrees with data in Fig. 19(b).

We can calculate the average number of particles in the lattice from the derived distribution. The total number of order-1 peaks is

$$\begin{aligned} K &= 2 \int_0^{L/2} W(x) dx = 2\sqrt{2} \int_w^c \frac{W dW}{\sqrt{W^4 - w^4}} \\ &= \sqrt{2} \int_1^{c^2 w^{-2}} \frac{dy}{\sqrt{y^2 - 1}} = 2^{1/2} \ln(y + \sqrt{y^2 - 1}) \Big|_1^{c^2 w^{-2}} \\ &\approx 2^{3/2} \ln L, \end{aligned}$$

where in the last expression we assumed $w \ll 1$ and neglected $\ln c\pi$. The numerical dependence of K on $\ln L$ is presented in Fig. 20.

-
- [1] Z. Warhaft, Passive scalars in turbulent flows, *Annu. Rev. Fluid Mech.* **32**, 203 (2000).
- [2] R. H. Kraichnan, Anomalous scaling of a randomly advected passive scalar, *Phys. Rev. Lett.* **72**, 1016 (1994).
- [3] T. Elperin, N. Kleeorin, and I. Rogachevskii, Dynamics of the passive scalar in compressible turbulent flow: Large-scale patterns and small-scale fluctuations, *Phys. Rev. E* **52**, 2617 (1995).
- [4] A. Vulpiani, F. Cecconi, and M. Cencini, *Chaos: From Simple Models to Complex Systems* (World Scientific, Singapore, 2009), Vol. 17.
- [5] J. M. Deutsch, Probability distributions for multicomponent systems with multiplicative noise, *Physica A* **208**, 445 (1994).
- [6] S. Lepri, Fluctuations in a diffusive medium with gain, *Phys. Rev. Lett.* **110**, 230603 (2013).
- [7] E. Schröder, J. S. Andersen, M. T. Levinsen, P. Alstrøm, and W. I. Goldburg, Relative particle motion in capillary waves, *Phys. Rev. Lett.* **76**, 4717 (1996).
- [8] G. Ricard and E. Falcon, Experimental quasi-1d capillary-wave turbulence, *Europhys. Lett.* **135**, 64001 (2021).
- [9] F. Leyvraz, Scaling theory and exactly solved models in the kinetics of irreversible aggregation, *Phys. Rep.* **383**, 95 (2003).
- [10] A. S. Pikovsky, Synchronization and stochastization of the ensemble of autogenerators by external noise, *Radiophys. Quantum Electron* **27**, 390 (1984).
- [11] V. A. Antonov, Modeling of processes of cyclic evolution type. Synchronization by a random signal, *Proc. Leningrad Univ., Astron.* (in Russian) **67** (1984).
- [12] H. Crauel and F. Flandoli, Attractors for random dynamical systems, *Probab. Theor. Relat. Fields* **100**, 365 (1994).
- [13] Z. F. Mainen and T. J. Sejnowski, Reliability of spike timing in neocortical neurons, *Science* **268**, 1503 (1995).
- [14] P. Khoury, M. A. Lieberman, and A. J. Lichtenberg, Experimental measurement of the degree of chaotic synchronization using a distribution exponent, *Phys. Rev. E* **57**, 5448 (1998).
- [15] A. Uchida, R. McAllister, and R. Roy, Consistency of nonlinear system response to complex drive signals, *Phys. Rev. Lett.* **93**, 244102 (2004).
- [16] A. S. Pikovsky, Statistics of trajectory separation in noisy dynamical systems, *Phys. Lett. A* **165**, 33 (1992).
- [17] J. C. Sommerer and E. Ott, Particles floating on a moving fluid: a dynamically comprehensible physical fractal, *Science* **259**, 335 (1993).
- [18] K. Gawedzki and M. Vergassola, Phase transition in the passive scalar advection, *Physica D* **138**, 63 (2000).
- [19] T. Bohr and A. S. Pikovsky, Anomalous diffusion in the Kuramoto-Sivashinsky equation, *Phys. Rev. Lett.* **70**, 2892 (1993).
- [20] X.-H. Wang and K.-L. Wang, Analysis of anomalous diffusion in the Kuramoto-Sivashinsky equation, *Phys. Rev. E* **49**, 5853 (1994).
- [21] S. F. Edwards and D. R. Wilkinson, The surface statistics of a granular aggregate, *Proc. R. Soc. London* **A381**, 17 (1982).
- [22] M. Kardar, G. Parisi, and Y.-C. Zhang, Dynamic scaling of growing interfaces, *Phys. Rev. Lett.* **56**, 889 (1986).
- [23] D. Das and M. Barma, Particles sliding on a fluctuating surface: Phase separation and power laws, *Phys. Rev. Lett.* **85**, 1602 (2000).
- [24] B. Drossel and M. Kardar, Passive sliders on growing surfaces and advection in Burger's flows, *Phys. Rev. B* **66**, 195414 (2002).
- [25] D. Das, M. Barma, and S. N. Majumdar, Fluctuation-dominated phase ordering driven by stochastically evolving surfaces: Depth models and sliding particles, *Phys. Rev. E* **64**, 046126 (2001).
- [26] C.-S. Chin, Passive random walkers and riverlike networks on growing surfaces, *Phys. Rev. E* **66**, 021104 (2002).
- [27] A. Nagar, S. N. Majumdar, and M. Barma, Strong clustering of noninteracting, sliding passive scalars driven by fluctuating surfaces, *Phys. Rev. E* **74**, 021124 (2006).
- [28] T. Singha and M. Barma, Clustering, intermittency, and scaling for passive particles on fluctuating surfaces, *Phys. Rev. E* **98**, 052148 (2018).
- [29] V. Zakharov, F. Dias, and A. Pushkarev, One-dimensional wave turbulence, *Phys. Rep.* **398**, 1 (2004).

- [30] A. Majda, D. McLaughlin, and E. Tabak, A one-dimensional model for dispersive wave turbulence, *J. Nonlin. Sci.* **7**, 9 (1997).
- [31] F. Cagnetta, M. R. Evans, and D. Marenduzzo, Statistical mechanics of a single active slider on a fluctuating interface, *Phys. Rev. E* **99**, 042124 (2019).
- [32] K. Kang and S. Redner, Fluctuation effects in Smoluchowski reaction kinetics, *Phys. Rev. A* **30**, 2833 (1984).
- [33] H. Takayasu and Y-h. Taguchi, Non-Gaussian distribution in random advection dynamics, *Phys. Rev. Lett.* **70**, 782 (1993).
- [34] C. Kipnis, C. Marchioro, and E. Presutti, Heat flow in an exactly solvable model, *J. Stat. Phys.* **27**, 65 (1982).
- [35] R. Rajesh and S. N. Majumdar, Conserved mass models and particle systems in one dimension, *J. Stat. Phys.* **99**, 943 (2000).
- [36] S. Krishnamurthy, R. Rajesh, and O. Zaboronski, Persistence properties of a system of coagulating and annihilating random walkers, *Phys. Rev. E* **68**, 046103 (2003).
- [37] Our notation is different from the notation of the original paper [33] that employed the parameter $j = 1 - \epsilon$. Our choice is due to our interest in the limit $\epsilon \rightarrow 0$.
- [38] At first glance, this statement is not obvious because the limit $\epsilon \rightarrow 1$ might not commute with the thermodynamic limit $L \rightarrow \infty$. However, we will provide a consistent description for any L and ϵ .
- [39] M. Takayasu, H. Takayasu, and Y. Taguchi, Non-Gaussian distribution in random transport dynamics, *Int. J. Mod. Phys. B* **08**, 3887 (1994).
- [40] H. Takayasu, T. Kawakami, Y. Taguchi, and T. Katsuyama, Fractal limit distributions in random transports, *Fractals* **04**, 257 (1996).
- [41] S. Ispolatov, P. L. Krapivsky, and S. Redner, Wealth distributions in asset exchange models, *Eur. Phys. J. B* **2**, 267 (1998).
- [42] A. Dragulescu and V. M. Yakovenko, Statistical mechanics of money, *Eur. Phys. J. B* **17**, 723 (2000).
- [43] E. Heinsalu and M. Patriarca, Kinetic models of immediate exchange, *Eur. Phys. J. B* **87**, 170 (2014).
- [44] B. van Ginkel, F. Redig, and F. Sau, Duality and stationary distributions of the immediate exchange model and its generalizations, *J. Stat. Phys.* **163**, 92 (2016).
- [45] M. F. Barnsley, *Fractals Everywhere* (Academic, London, 2014).
- [46] The implementation of the latter property explains why we choose m/L rather than t/L^2 as the second argument of $F_2(x, y)$.
- [47] F. Family and T. Vicsek, Scaling of the active zone in the Eden process on percolation networks and the ballistic deposition model, *J. Phys. A* **18**, L75 (1985).
- [48] T. Sun, H. Guo, and M. Grant, Dynamics of driven interfaces with a conservation law, *Phys. Rev. A* **40**, 6763 (1989).
- [49] J. Krug, Origins of scale invariance in growth processes, *Adv. Phys.* **46**, 139 (1997).
- [50] F. Caballero, C. Nardini, F. van Wijland, and M. E. Cates, Strong coupling in conserved surface roughening: A new universality class?, *Phys. Rev. Lett.* **121**, 020601 (2018).
- [51] N. R. Smith, B. Meerson, and P. V. Sasorov, Local average height distribution of fluctuating interfaces, *Phys. Rev. E* **95**, 012134 (2017).
- [52] S. N. Majumdar, S. Krishnamurthy, and M. Barma, Nonequilibrium phase transitions in models of aggregation, adsorption, and dissociation, *Phys. Rev. Lett.* **81**, 3691 (1998).
- [53] R. Rajesh and S. N. Majumdar, Exact phase diagram of a model with aggregation and chipping, *Phys. Rev. E* **63**, 036114 (2001).
- [54] E. Falcon and N. Mordant, Experiments in surface gravity-capillary wave turbulence, *Annu. Rev. Fluid Mech.* **54**, 1 (2022).
- [55] Y. Peres, W. Schlag, and B. Solomyak, Sixty years of Bernoulli convolutions, in *Fractal Geometry and Stochastics II* (Birkhäuser, Basel, 2000), pp. 39–65.
- [56] S. J. Fraser and R. Kapral, Periodic dichotomous-noise-induced transitions and stochastic coherence, *Phys. Rev. A* **45**, 3412 (1992).
- [57] R. Kapral and S. J. Fraser, Dynamics of oscillators with periodic dichotomous noise, *J. Stat. Phys.* **70**, 61 (1993).
- [58] Y. Peres, K. Simon, and B. Solomyak, Absolute continuity for random iterated function systems with overlaps, *J. London Math. Soc.* **74**, 739 (2006).
- [59] J. Barral and D.-J. Feng, On multifractal formalism for self-similar measures with overlaps, *Math. Z.* **298**, 359 (2021).
- [60] A. Pikovsky and L. S. Tsimring, Statistical theory of asymmetric damage segregation in clonal cell populations, *Math. Biosci.* **358**, 108980 (2023).